Mon. Not. R. Astron. Soc. **342,** 1241–1259 (2003)

Brown dwarfs and low-mass stars in the Pleiades and Praesepe: membership and binarity

D. J. Pinfield,[1⋆] P. D. Dobbie,[2] R. F. Jameson,[2] I. A. Steele,[1]
H. R. A. Jones[1] and A. C. Katsiyannis[3]

[1]*Astrophysics Research Institute, Liverpool John Moores University, 12 Quays House, Egerton Wharf, Birkenhead CH41 1LD*
[2]*Department of Physics & Astronomy, University of Leicester, University Road, Leicester LE1 7RH*
[3]*Department of Pure & Applied Physics, The Queen's University of Belfast, Belfast BT7 1NN*

Accepted 2003 March 12. Received 2003 March 10; in original form 2002 September 11

ABSTRACT

We present near-infrared J-, H- and K-band photometry and optical spectroscopy of low-mass star and brown dwarf (BD) candidates in the Pleiades and Praesepe open clusters. We flag non-members from their position in K, $I-K$ and J, $J-K$ colour–magnitude diagrams (CMDs), and $J-H$, $H-K$ two-colour diagrams. In general, the dust-free NextGen model isochrones of the Lyon Group fit the K, $I-K$ CMDs well for stars with $I-K \sim 1.5$–3.5. However, Pleiades stars with $K \simeq 10.5$–13 ($M_K \simeq 5$–7.5) are rather redder than the isochrones. We also identify this effect amongst αPer sources from the literature, but find no evidence of it for field stars from the literature. The NextGen isochrones fit the J, $J-K$ CMDs of both clusters very well in this photometric range. It is possible that the $I-K$ colour of youthful stars is affected by the presence of magnetic activity. The Lyon Group's Dusty isochrones fit both K, $I-K$ and K, $J-K$ Pleiades CMDs well for $I-K \simeq 4.3$–$6/J-K \simeq 1.1$–1.4. In between these colour ranges the Pleiades cluster sequence comprises three portions. Starting at the bluer side, there is a gap where very few sources are found (the gap size is $\Delta I \sim 0.5$, $\Delta J \sim \Delta K \sim 0.3$), probably resulting from a sharp local drop in the magnitude–mass relation. Then the sequence is quite flat from $I-K \sim 3.5$–4. Finally, the sequence turns over and drops down to join the Dusty isochrone. We also compare model atmosphere colours to the two-colour diagrams of the clusters. The NextGen models are seen to be ∼0.1 too blue in $H-K$ and ∼0.1 too red in $J-H$ for $T_{\rm eff} > 4000$ K. However, they are in reasonable agreement with the data at $T_{\rm eff} \sim 3200$ K. For $T_{\rm eff} \sim 2800$–3150 K, the colours of Pleiades and Praesepe sources are significantly different, where Praesepe sources are ∼0.1 bluer in $J-H$ and up to ∼0.1 redder in $H-K$. These differences could result from gravity-sensitive molecular opacities. Cooler Praesepe sources then agree well with the dusty models, suggesting that dust is beginning to form in Praesepe sources around 2500 K. However, Pleiades sources remain consistent with the NextGen models (and inconsistent with the dusty models) down to $T_{\rm eff}$ values of ∼2000 K. It is possible that dust formation does not begin until lower $T_{\rm eff}$ values in sources with lower surface gravities (and hence lower atmospheric pressures). We also identify unresolved binaries in both clusters, and estimate mass ratios (q) for Pleiades BDs. Most of these have $q > 0.7$, however, 3/18 appear to have lower q values. We determine the binary fraction (BF) for numerous mass ranges in each cluster, and find that it is generally rising towards lower masses. We find a BD BF of 50^{+11}_{-10} per cent. We also find some evidence suggesting that the BF–q distribution is flat for 0.5–0.35 $M_\odot$, in contrast to solar-type stars.

Key words: stars: low-mass, brown dwarfs – open clusters and associations: individual: Pleiades Praesepe.

⋆E-mail: dpi@astro.livjm.ac.uk

1 INTRODUCTION

Low-mass star and brown dwarf (BD) populations in open clusters make excellent test-beds for our theoretical understanding of these objects. With a well-constrained cluster age, and assuming uniform composition, we can effectively compare theoretical isochrones with observed colour–magnitude diagrams (CMDs) and two-colour diagrams without the complications introduced by a spread in metallicity and a range in surface gravities for a given mass. Furthermore, for most open clusters, the depth effect is small, and the single star sequence is therefore quite tight on CMDs. It is thus possible to study unresolved binarity amongst cluster members.

The $T_{\rm eff}$ range of young to intermediate age low-mass stars and BDs corresponds to *M* and *L* spectral types, and modelling the atmospheres of such objects is very complicated. The convection zone penetrates deeply into the optically thin outer layers due to H_2 dissociation (Burrows et al. 1993). Molecular opacities such as TiO and H_2O comprise millions of lines that must be accurately modelled (Allard et al. 1997). Also, dust begins to form in atmospheres at around 2800 K (Allard et al. 2001), which depletes opacities as well as affecting the atmospheric temperature gradient. There are many different varieties of dust (Sharp & Huebner 1990), and their formation rates and grain size distributions will depend not only on temperature, but on surface gravity and metallicity. Despite these complexities, much progress has been made in modelling these atmospheres. The Lyon Group has combined structural models (using interior structure physics) with model atmospheres (Hauschildt, Allard & Baron 1999; Allard et al. 2001) to calculate evolutionary models for low-mass stars and BDs, both with and without atmospheric dust condensates (Baraffe et al. 1998, hereafter NextGen; Chabrier et al. 2000, hereafter Dusty). Calculations by other groups include those of Burrows et al. (1997), and D'Antona & Mazzitelli (1994). However, only the Lyon group models are based on consistent non-grey evolutionary calculations relating the mass and age of an object to its observational properties (colour and magnitude).

The Pleiades and Praesepe are two nearby, rich open clusters with near solar composition (Crawford & Perry 1976; Hambly et al. 1995b). With distances of ∼125 and 160 pc, respectively, both clusters have small depth effects, and are fairly compact on the sky (a few degrees across). The Pleiades is ∼125 Myr old (Stauffer, Schultz & Kirkpatrick 1998) and Praesepe is ∼0.6–1.4 Gyr old (Hambly et al. 1995b). Consequently, Pleiades low-mass stars ($\leqslant 0.3$ $M_\odot$) and BDs are not fully contracted, and will have lower surface gravities than their equal $T_{\rm eff}$ counterparts in Praesepe.

In this paper, we derive membership criteria of Pleiades and Praesepe low-mass star and BD candidates using near-infrared (NIR) photometry and optical spectroscopy. We compare NextGen and Dusty theoretical isochrones to our observed CMDs and two-colour diagrams, and identify photometric ranges where the isochrones agree well with observations. We then join these isochrone sections together using additional empirical points, and discuss the overall form of the cluster sequences. We also use our CMDs and two-colour diagrams to identify unresolved binaries. We derive binary fractions over several mass ranges in each cluster, and estimate mass ratios for the Pleiades BD binaries. Finally, we discuss future work.

2 OBSERVATIONS AND DATA REDUCTION

2.1 The Pleiades and Praesepe samples

Our Pleiades and Praesepe samples were taken from several sources. For the Pleiades, the highest-mass sources ($I < 13.5$) were taken from Hambly, Hawkins & Jameson (1993, HHJ hereafter). Fainter sources were taken from, the ITP survey (Zapatero-Osorio et al. 1999), the CFHT survey (Bouvier et al. 1998), the Burrell Schmidt survey (Pinfield et al. 2000, BPL hereafter) and the INT WFC survey (Dobbie et al. 2002b). The fainter surveys cover a combined area of 7.6 deg^2, and range in photometric depth from $I = 19.5$ to 21.8 (unless otherwise stated, *I* refers to Cousins *I*). These fainter surveys are summarized in more detail in Jameson et al. (2002).

Our Praesepe sample was taken from four surveys. Proper motion members from the 19 deg^2 survey of Hambly et al. (1995a, hereafter HSHJ) represent our highest mass sources ($I = 10$–17.5). Lower-mass sources come from Pinfield et al. (1997), Pinfield (1997) and Magazzu et al. (1998). The Pinfield surveys covered 1 and 6 deg^2, and reached $I = 21$ and 19.5, respectively. The Magazzu survey covered 800 arcmin^2 down to $I = 21.2$, and identified one BD candidate, which they called Roque Pr 1.

2.2 Photometry

For the brighter BPL and HSHJ candidates we obtained *J*-, *H*- and *K*-band magnitudes from the 2MASS second incremental point-source catalogue at the NASA/IPAC InfraRed Science Archive (Scrutskie et al. 1995). We used a search radius of 3 arcsec to allow for positional uncertainties. For the ITP, CFHT and INT WFC surveys, we obtained photometry from the literature for as many sources as were available (see Jameson et al. 2002). Most of the fainter BPL candidates had *K*-band measurements from Pinfield et al. (2000), and several Praesepe candidates had *K*-band measurements from Hodgkin et al. (1999). For the remainder of these samples we measured *J*-, *H*- and *K*-band photometry using UFTI on the United Kingdom Infrared Telescope (UKIRT) on Mauna Kea, Hawaii, from 2000 January 3 to 5, and in service time on 2001 October 8. The sky conditions were photometric. Our observing strategy for candidates without a *K*-band magnitude was to observe them first at *K*, and only go on to measure *J*- and *H*-band magnitudes if the targets had a sufficiently red $I - K$ colour to be consistent with membership of the cluster. For the remaining candidates, we simply measured *J*- and *H*-band magnitudes, as well as *K* band if the previous *K* uncertainty was >0.1. Each observation comprised a five-point dither pattern, with a windowed 512 × 512 pixel readout. Total integration times at each of *J*, *H* and *K* were 150, 300 and 540 s, for objects with $I = 17$–18.5, $I = 18.5$–20 and $I > 20$, respectively. The raw images were de-biased, dark-subtracted, flat-fielded and combined into mosaics using ORACDR. Aperture photometry was then extracted using GAIA. As the UKIRT photometry was obtained with the 'Mauna Kea Observatory' (MKO) filter set (Simons & Tokunaga 2002), the photometry from the literature was transformed into the MKO system using the transforms of Hawarden et al. (2001) and Carpenter (2001) (old UKIRT system and 2MASS, respectively). The photometry is given in the appendices. Where there were multiple measurements available for an object, we selected those with small errors (generally trying to avoid measurements with errors larger than ∼0.1), and took an average.

Our optical photometry was taken from the literature. All *I*-band photometry was transformed into the Cousins system. Photographic I_N magnitudes from HSHJ were transformed using Bessell (1986). To transform the $I_{\rm KP}$ magnitudes of Pinfield (1997) and Pinfield et al. (2000) we derived the following relation: $I_{\rm C} - I_{\rm KP} = 0.049\,(I_{\rm KP} - K) + 0.069$ (for $2.3 < I_{\rm C} - K < 5.8$). This relation was obtained using synthetic photometry derived from spectra, using the method and data from Dobbie et al. (2002a).

2.3 Spectroscopy

We obtained spectra of two BD candidates using ISIS on the 4.2-m William Herschel Telescope (WHT) during 2001 January 29. The seeing was ∼1.2 arcsec and the weather was clear. Our instrumental setup comprised the TEK4 charge-coupled device (CCD) and the R158R grating on the ISIS red arm, with the mirror in place and no order blocking filters, so as to minimize flux losses (we expect second-order contamination for these red objects to be negligible). We used a 1-arcsec slit, and integrated for 1800 s. This gave us a wavelength coverage of 6213–9193 Å with a dispersion of 2.91 Å pixel^{-1}.

We used IRAF to reduce our spectra. The CCD frames were bias-subtracted and flat-fielded using standard routines, and the spectra extracted and sky-subtracted using the APALL routine. We calibrated the wavelength scale using the CuAr arc lamp exposures, and the flux using observations of flux standard stars (available in the IRAF environment) on the same night, and with the same instrumental setup.

3 RESULTS AND DISCUSSION

3.1 Pleiades spectra

Fig. 1 shows the spectra of the two Pleiades BD candidates BPL 327 and BPL 45, where they have been normalized to unity at 7500 Å. Table 1 shows the spectroscopic information extracted from these data. Our adopted spectral types were derived using the pseudo-continuum ratio PC3 from Martín, Rebolo & Zapatero-Osorio (1996), and have uncertainties of ±0.5. For BPL 327 the VO index of Kirkpatrick, Henry & Simons (1995) agrees with the PC3 index. Also, the A-index of Kirkpatrick, Henry & McCarthy (1991) implies a slightly earlier spectral type for both sources (dM6.5 and dM7.5 for BPL 327 and BPL 45, respectively), which is what we expect for young sources that are not fully contracted. We also note that the BPL 327 spectra shows that the I2 and I3 indices of Martín & Kun (1996) (which measure the CaH and the TiO absorption bands, respectively) continue to increase out to ∼dM7, before turning over and decreasing to lower values by dM8. By comparing the I magnitudes and derived spectral types with the spectral type-magnitude diagram of Martín et al. (2000), we found that both BPL 327 and BPL 45 lie on the Pleiades sequence, and appear to be single BDs.

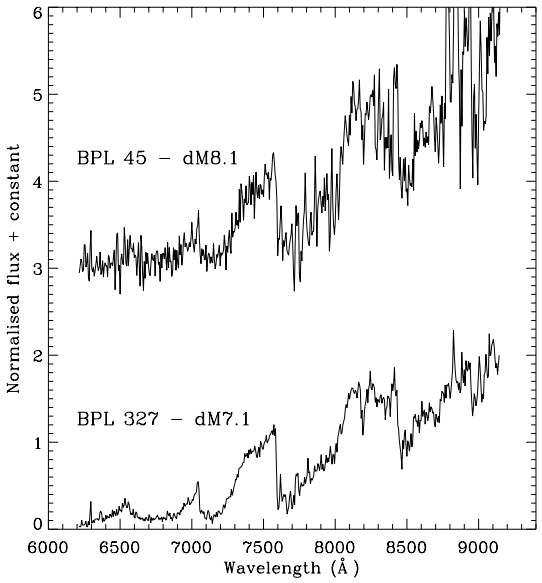

Figure 1. The two Pleiades BD candidate spectra (normalized to unity at 7500 Å). The noisier spectra of BPL 45 has been binned by 2 pixel in this plot and offset for clarity.

3.2 The *IK* CMDs

Figs 2 and 3 show the K, $I-K$ CMDs (*IK* CMDs) for the Pleiades and Praesepe, respectively. Small filled circles are higher-mass candidate members with 2MASS photometry, and proper motion candidates from HSHJ in the Pleiades and Praesepe, respectively. We have several additional fainter Praesepe candidates with 2MASS photometry which are not plotted, since their errors are sizeable (see Table A4). Larger filled symbols are lower mass candidates (candidate BDs in the Pleiades), where circles have J- and H-band photometry (triangles do not). Open circles (small and large) look like background sources in these plots. Open diamonds and open squares are probably old-disc non-members from the K, $J-K$ CMDs (*JK* CMDs) and the $J-H$, $H-K$ two-colour diagrams (*JHK* diagrams), respectively (see Sections 3.4 and 3.5). Circled objects look like unresolved binaries in these plots (see below). Objects overplotted with an additional square or triangle are likely to be unresolved binaries from the *JK* CMDs and *JHK* diagrams. Typical photometric error bars are shown at the bottom left. The location of several magnitude bins are indicated with dotted lines (see Section 3.5). Solar metallicity NextGen and Dusty isochrones are overplotted as dashed lines, with mass points shown in units of 0.001 $M_\odot$. We also show higher-mass (>0.7 $M_\odot$) isochrones derived with a larger mixing length parameter ($l = 1.9H_p$), since this parameter makes a significant difference at these higher masses (Chabrier & Baraffe 1997). In the Pleiades, we assume an age of 125 Myr, $A_I = 0.06$, $A_K = 0.05$, and use the re-computed *Hipparcos* distance modulus of $(m-M)_0 = 5.57$ (Makarov 2002), which was derived in a way that reduces the propagation of along-scan attitude errors, a source of discrepancy with the previous *Hipparcos* Pleiades distance (e.g. van Leeuwen 1999). In Praesepe, we show both 0.5- and 1-Gyr isochrones, and assume $(m-M)_0 = 6.0$ with zero extinction. This distance modulus was obtained from a best fit of the NextGen isochrones to the good Praesepe candidates with UKIRT photometry from $I-K = 2.5$ to 3.5. In this colour range the 0.5- and 1-Gyr isochrones lie on top of each other. This distance agrees well with other values found from main-sequence fitting (Lynga 1987; Nissen 1988), but is slightly lower than the *Hipparcos* value of 6.24 (Mermilliod et al. 1997). However, it is possible that the previously mentioned attitude errors could affect the *Hipparcos* distance of Praesepe. The overplotted solid lines represent our selected

Table 1. Spectral indices and equivalent widths of the Pleiades BD candidates.

Source	SpT	PC3	A	VO	I3	I2	H_αEW (Å)	KI 7655 EW (Å)	KI 7699 EW (Å)	Na I 8183+8195 EW (Å)
BPL 327	dM7.1	1.55	1.52	2.45	2.33	1.03	-5 ± 2	-12 ± 3	-10 ± 3	-7 ± 1
BPL 45	dM8.1	1.76	1.69	–	–	–	–	–	–	-7 ± 2

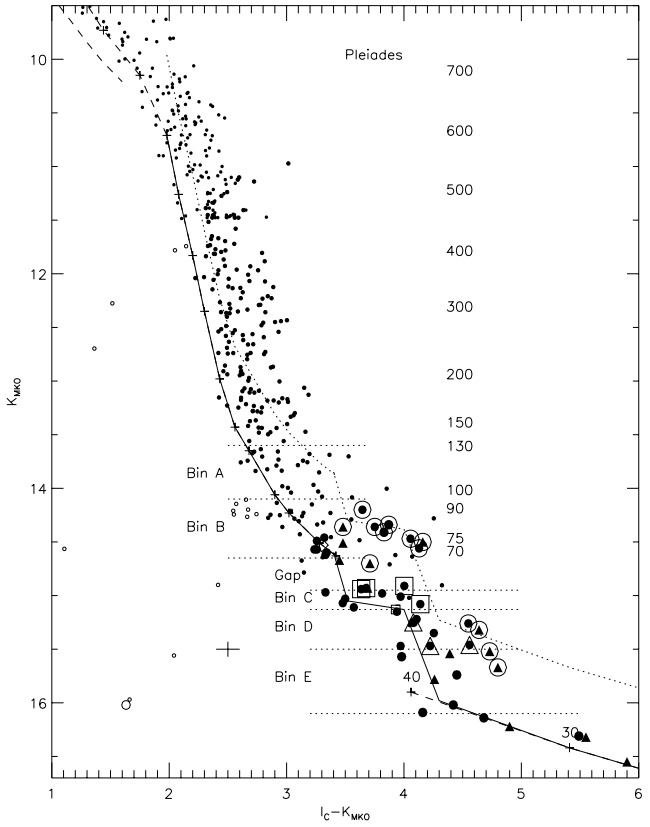

Figure 2. The K, $I-K$ CMD of the Pleiades. Small filled circles have 2MASS photometry. Larger filled symbols have UKIRT photometry; circles have *JHK*, triangles have just K. Open circles are non-members. Circled objects are *IK* binaries. Objects overplotted with an additional open square or triangle are *JK* or *JHK* binaries, respectively (see the text). Dashed lines are the NextGen and Dusty models. Solid and dotted lines are the cluster single and binary star sequences, respectively.

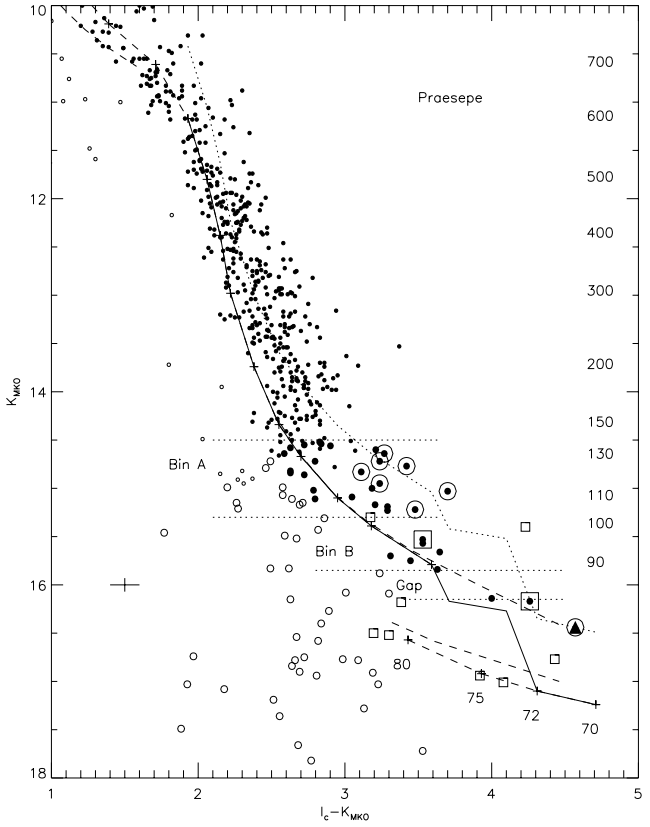

Figure 3. The K, $I-K$ CMD of Praesepe. Symbols are the same as in Fig. 2.

cluster sequences (constructed both from isochrone data and empirical data), with their equal-mass binary sequences shown as dotted lines (see the subsequent discussion).

We will first discuss the brighter sources with 2MASS K-band photometry. For the range $K = 10.5$–14 in the Pleiades and $K =$ 11–14.5 in Praesepe there is a known kink in the main sequence, where it becomes steeper. This feature is seen over a wide range of wavelengths (Reid & Cruz 2002), and is thought to result from H_2 formation in the photosphere, lowering the adiabatic gradient and causing convection (Kroupa, Tout & Gilmore 1990). The resulting lower-temperature gradient then leads to increased $T_{\rm eff}$ values, with the consequent reduction in the $I-K$ colour, and turn over on the CMD. The kink is clearly seen in both cluster CMDs. For Praesepe, the model isochrone follows the data very well (to within the photometric errors). However, for the Pleiades the data appear to be somewhat redder than the isochrones from $K = 10.5$–13 ($M_K \sim 5$–7.5). In order to determine whether this effect is an artefact of the different photometric filter systems used, we have examined our photometry more closely. Photographic magnitudes (used in HHJ) and KittPeak magnitudes (used in Pinfield et al. 2000) were both available for the Pleiades sources in this range, and by transforming both on to the Cousins system we looked for any systematic differences that could account for such an effect. However, no such differences were found, and the Pleiades sources looked redder than the isochrones whichever I-band data were used. The Pleiades and Praesepe sources in this range all have 2MASS K-band photometry (converted on to the MKO system), and so there should be no systematic difference in this band. It thus seems unlikely that this effect is due to photometric inconsistencies.

Assuming this effect is genuine, we should expect to see it amongst other similar populations. The open cluster αPer has a similar age to the Pleiades ($\simeq$80 Myr), and Fig. 4 shows an *IK* CMD of likely αPer members (filled circles) from Prosser (1992) and Barrado y Navascués et al. (2002). These have been corrected for distance and reddening ($m - M = 6.23$, $A_I = 0.17$, $A_K = 0.04$; Stauffer et al. 1999) for easy comparison with the field stars that are also plotted (open circles; Reid & Cruz 2002). NextGen isochrones of 80 Myr and 1 Gyr are indicated by solid lines, and a dotted line indicates the expected spread due to binarity for αPer. It is clear that (despite some scatter) the 1-Gyr model isochrones represent the field star data very well. However, the majority of the αPer sources from $M_K \sim 5$–7 are redder than both the single and the binary 80-Myr isochrones, and the same effect is therefore evident in αPer as well as the Pleiades.

So what could be causing this reddening? Variability could make a source appear redder since the I- and K-band measurements were not made simultaneously. However, sources could equally be flaring when the I- or K-band measurements were made, and the overall effect should be to simply broaden the sequence slightly, not shift it to the red. The magnetic activity of such youthful sources may, however, provide the explanation for the reddening. Hawley, Tourtellot & Reid (1999) found that dMe stars in NGC 2516 (~Pleiades age) lay redward of the fiducual main sequence in an M_V versus $V-I$ CMD. They also found that some molecular bands respond strongly

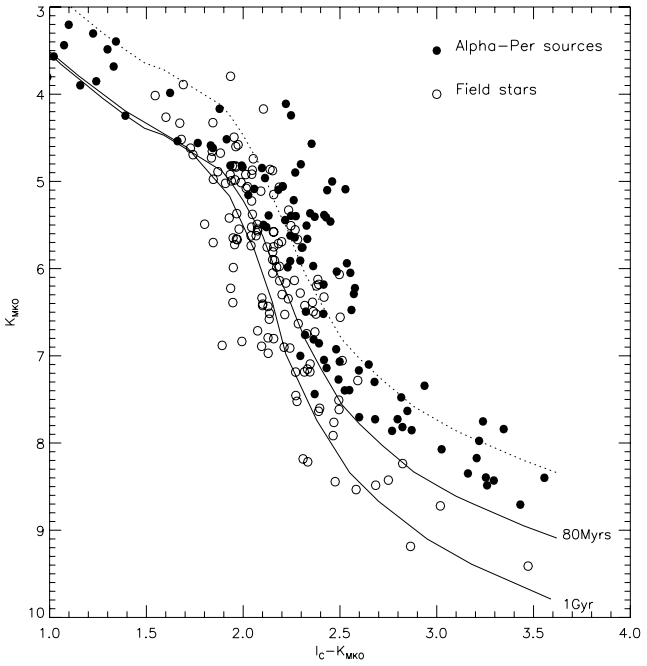

Figure 4. The K, $I-K$ CMD of Alpha-Per (filled circles) and field stars (open circles). Sources are taken from Prosser (1992), Barrado y Navascués et al. (2002), and Reid & Cruz (2002).

to the presence of a chromosphere, and concluded that the $V-I$ colour was affected by the presence of activity. The $I-K$ colour and the $V-I$ colour could be reddened by the same process. It may seem surprising that photospheric bands (and the photometric colours they influence) should be affected by the presence of a chromosphere. However, modelling the correct form of the magnetic field that threads the atmospheres of these stars may allow us to account for these effects.

Below the kink the NextGen isochrone fits both cluster CMDs well out to $I-K\sim3.5$, showing the expected decreasing $T_{\rm eff}$ as degeneracy sets in. For Praesepe, we defined our cluster sequence out to $I-K\simeq3.5$ with the NextGen model isochrone, since it fits the data very well in this range. We chose to do the same for the Pleiades despite the sources being slightly redder than the isochrones for $K=10.5$–13, since we do not expect the reddening to significantly effect the mass–magnitude model predictions.

At redder colours we confine our discussion to the Pleiades, since we only have a few good Praesepe candidates in this range. It can be seen that there is a fairly obvious gap in the Pleiades sequence from $K\simeq14.65$ to 14.95 (at $I-K\simeq3.5$) where the number of sources is severely reduced. The spectral type corresponding to the gap is M7 (see fig. 4 of Martín et al. 2000), and we refer to this feature as the 'M dwarf gap'. It is discussed in more detail in Dobbie et al. (2002c). However, to summarize, we believe that it results from a sharp local drop in the magnitude–mass relation, possibly caused by the formation of dust in the atmospheres of objects in this $T_{\rm eff}$ regime. We measured the size of the gap at 0.3 in K, which compares with ∼0.5 in I (Dobbie et al. 2002c).

Below the Pleiades M dwarf gap ($K\simeq14.95$–15.3) the single-source candidates follow a fairly flat path in the CMD out to $I-K\sim4.1$. There is then a turn down, where the candidates drop on to the Dusty isochrone, joining it somewhere from $I-K\sim4.1$ to 4.5. We estimated the path followed by the flat part of the sequence by averaging the colours and K-band magnitudes of two groups of sources; the three bluest single sources and the three reddest single sources from $K=14.95$–15.3 (below which the turn down is obvious). And we estimated the colour where the sequence joins the Dusty isochrone as $I-K\sim4.3$. The Dusty isochrone then agrees well with the five faintest Pleiades candidates out to $I-K\sim6$, so in this range we used the Dusty isochrones for our sequence.

For Praesepe, we have extended the cluster sequence beyond the NextGen isochrones by assuming it has the same form as the Pleiades sequence; the same M dwarf gap size, and the same flat portion that turns over and falls on to the Dusty isochrone by $I-K\sim4.3$. This may not be entirely accurate, but should act as a reasonable approximation.

We have flagged non-members in the Pleiades and Praesepe using our cluster sequences as a guide, and allowing for photometric uncertainties as well as the depth effect of the clusters (±0.2 mag for the Pleiades and ±0.15 mag for Praesepe; Pinfield, Jameson & Hodgkin 1998; Holland et al. 2000). We have also flagged likely unresolved binary members with UKIRT photometry, if they lie significantly (>0.25 mag) above the single-star sequence. We duly identified 13 Pleiades binaries and eight Praesepe binaries in this way. We refer to them as *IK* binaries, and they are overplotted with an open circle in the figures. We note that there is a degeneracy between mass and binarity where the *IK* sequence is dropping down on to the Dusty isochrone ($I-K=3.9$–4.5), and it is not possible to identify all binaries in this region from the *IK* CMD alone.

3.3 Model $J-K$ colours

In the previous section we found that the NextGen isochrones fit the *IK* CMDs very well for $I-K\sim1$–3.5, except for Pleiades sources from $K=10.5$–13, which are slightly redder than the isochrones. We also found that Dusty isochrones fit the Pleiades *IK* CMD well for $I-K=4.3$–6. In this section we test the $J-K$ model predictions for these ranges, for a sample of field stars with kinematics and well measured $I-K$ and $J-K$ colours.

Fig. 5 shows $J-K$ plotted against $I-K$ for sources taken from Leggett (1992), Leggett, Allard & Hauschildt (1998) and Dahn et al. (2002). All sources classified as young or old disc (from their kinematics) in the Leggett papers are shown as filled or open circles, respectively. In addition, we have assigned four L dwarfs as being young (<0.5 Gyr), based on lithium detections (Martín et al. 1999). These are also shown as filled circles. The uncertainties are generally ±0.05 in colour. We have also overplotted the NextGen and Dusty model isochrones for 120 Myr (dashed lines) and 1 Gyr (dotted lines).

Comparison of the two populations shows that for bluer sources ($I-K<3.5$, $J-K<1$), the old disc stars have a bigger spread in $J-K$ and on average are slightly bluer in $J-K$ than their young disc counterparts. The two NextGen isochrones essentially lie on top of each other in this range, and fit the data very well. For redder sources ($I-K=4.3$–6, $J-K=1.1$–2), the Dusty isochrones lie on top of each other, and are in excellent agreement with the young disc data. In between these two ranges the isochrones are all too blue in $J-K$. The NextGen models are too blue because they do not account for dust, and the Dusty models are too blue because they use a less sophisticated treatment of H_2O and TiO molecular opacities. This is all consistent with the gradual changeover from NextGen to Dusty isochrones that was seen in the *IK* CMDs, and suggests that these models should provide accurate NIR isochrones in the blue and red photometric ranges.

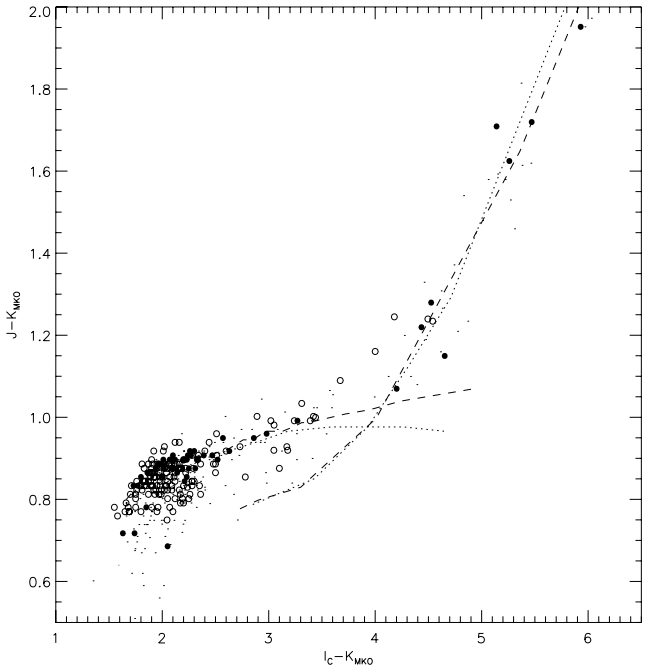

Figure 5. The $J - K$, $I - K$ two-colour diagram of field star sources. Filled circles are young disc, and open circles are old disc. Points have no age information available. 125 Myr and 1 Gyr NextGen and Dusty isochrones are shown as dashed and dotted lines, respectively.

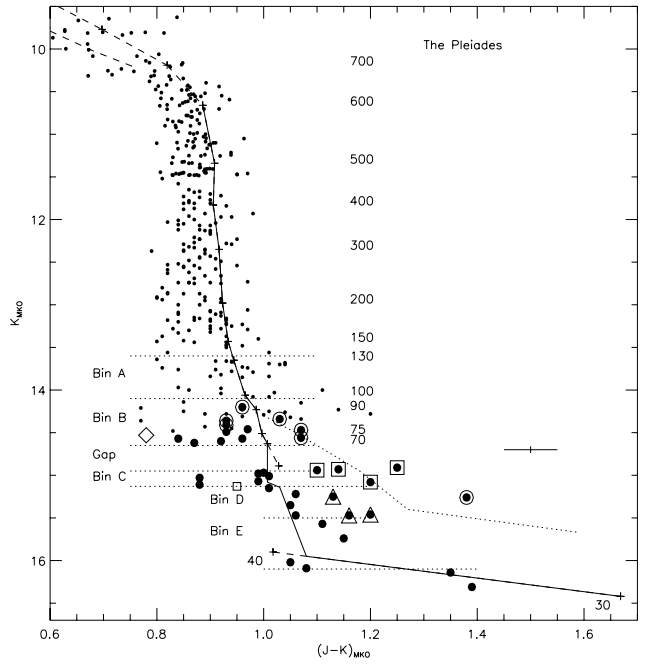

Figure 6. The K, $J - K$ CMD of the Pleiades. Symbols are the same as in Fig. 2.

3.4 The *JK* CMDs

Figs 6 and 7 show the *JK* CMDs for the Pleiades and Praesepe, respectively. Only good candidates from the *IK* CMDs are shown. The symbols mean the same as in Fig. 2. The location of several magnitude bins are indicated with dotted lines (see Section 3.5). Isochrones are overplotted as dashed lines, with mass points shown

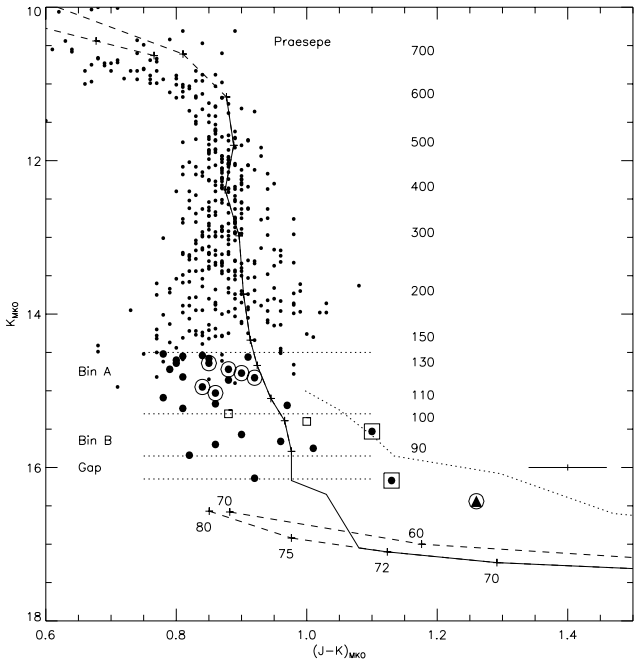

Figure 7. The K, $J - K$ CMD of Praesepe. Symbols are the same as in Fig. 2.

in units of 0.001 $M_\odot$. Typical photometric errors for UKIRT photometry are indicated.

We constructed cluster sequences for the *JK* CMDs based on our analysis in Sections 3.2 and 3.3. We used NextGen isochrones for $I - K < 3.5$ (mass > 0.07 and 0.09 $M_\odot$ for the Pleiades and Praesepe, respectively), and Dusty isochrones for $J - K = 1.1$–2 ($I - K = 4.3$–6). In between the NextGen and Dusty isochrones we added two additional sequence points, based on our Pleiades sources; one to bridge the M dwarf gap, and the other to represent the turn down point, where the sequences begins to fall on to the Dusty isochrone (see Section 3.2). An average of the $J - K$ colours of the Pleiades sources above and below the gap shows that there is essentially no significant $J - K$ colour change across the gap ($\Delta J - K = 0.01$). Averaging of the three single Pleiades sources in the turn down region gave a turn down colour of $J - K = 1.03$. The flat region seen in the *IK* CMDs is thus not very apparent in the *JK* CMDs. For Praesepe we assumed that the *JK* colour and magnitude changes are the same as in the Pleiades (as we did previously for the *IK* CMDs). The cluster sequences we constructed are shown as solid lines in the *JK* CMDs, and a dotted line indicates the spread we expect in the sequence from unresolved binarity.

The NextGen part of the sequence fits the observations very well in both clusters, and there is certainly no evidence for the Pleiades sources being redder than the isochrones from $K = 10.5$–13, as was seen in the *IK* CMDs. The $J - K$ colour is clearly not affected in the way that the $I - K$ colour is. Below the M dwarf gap, it can be seen that there is a spread in the Pleiades sources, where several are significantly redder than expected for single objects. A spread is also seen for a small number of Praesepe sources. Such a spread could result from several possibilities. Transient surface features such as spots could be responsible. The two most obvious red sources (Teide 1 and Calar 3; BPL 137 and 235) have been tested for variability. Bailer-Jones & Mundt (2001) found no evidence of *I*-band variability in Teide 1 over a 100-h time-scale, and only marginal evidence (just above the noise) for sporadic variability ($\Delta I < 0.03$) in Calar 3

over a 29-h time-scale. Our photometry of Teide 1 comprises three well-separated (>a year) J- and H-band measurements, which are consistent to within their errors. For Calar 3 we have one K-band measurement that is consistent with the measurement presented by Martín et al. (2000) and two H-band measurements that agree to within their errors. We also have three J-band measurements that show marginal evidence (at the 2σ level) of variability. The level of this variation is not in itself sufficient to account for the redness of Calar 3. Photometric errors will also cause some spread in the sources. However, the general consistency (at the 1σ level) between our multiple measurements makes it unlikely that these alone are responsible. The third option, and the one we chose to consider in more detail, is that additional unresolved binaries (not identified in the *IK* CMD) are present. A substantially redder unresolved companion could redden a source sufficiently to account for the spread. These binaries would either be background sources, or cluster binaries that come from the turn down region of the *IK* CMD, where binarity is not always apparent. We have thus flagged four additional candidate unresolved binaries in the Pleiades and two in Praesepe. We refer to these as *JK* binaries, and they are overplotted with an additional open square in the figures. We note that the bluest of the Pleiades *JK* binaries is a known background binary (without lithium; Martín et al. 2000), resolved by the *Hubble Space Telescope* (*HST*) (Martín et al. 1998). The Pleiades binaries will be discussed in more detail in Section 3.7. Of the two Praesepe *JK* binaries, the bluer one (RIZ Pr 23) is located just above where we expect the missing M dwarf gap to be, and could be a binary from below the gap. The redder one (RIZ Pr 23) comes from the turn down region of the *IK* CMD.

We have flagged non-members in the Pleiades and Praesepe using our cluster sequences as a guide. Objects that look too blue are presumably background stars from an old-disc population (see Section 3.3), and we flagged them as such if their $J - K$ colours were at least 2σ blueward of the cluster sequence.

3.5 The $J - H$, $H - K$ two-colour diagrams

Figs 8 and 9 show the $J - H$, $H - K$ two-colour diagrams (*JHK* diagrams) for the Pleiades and Praesepe, respectively. Only good candidates from the *IK* CMDs are shown. The source symbols mean the same as in Fig. 2. The positions of four field L dwarfs (from Dahn et al. 2002) are also shown as asterisks. The photometric error bars shown in the lower right-hand side of the plots are typical of the photometry of the BPL sources. The fainter sources have slightly larger errors. Solar metallicity model atmosphere predictions (used for the NextGen and Dusty models) are overplotted as dashed and solid lines, respectively, with labels indicating surface gravities. For the Pleiades we plot NextGen models for $T_{\rm eff} > 2000$ and 3000 K and Dusty models for $T_{\rm eff} < 2000$ K. For Praesepe, we plot NextGen models for $T_{\rm eff} > 2500$ and 3000 K, and Dusty models for $T_{\rm eff} < 2500$ K.

For the highest-mass stars, it can be seen that the NextGen models are ∼0.1 too blue in $H - K$ up to the two-colour turn-over, where convection begins (∼4000 K). The data turns over at $H - K = 0.27$, $J - H = 0.57$ and log g for such objects should be ∼4.5. The theoretical $J - H$ colour of the turn over is therefore ∼0.1 too red. These discrepancies are thought to be caused by inaccuracies in the modelling of water vapour opacities in the H band (with its overall low opacity) as well as an underestimation of the mixing length parameter. After the turn over, the 2MASS photometry follows a short path in the *JHK* diagram, reaching $J - H = 0.52$, $H - K = 0.38$ by ∼3200 K, in reasonable agreement with the log $g = 5$ NextGen model. In order to look for any non-evolutionary differences between the colours of Pleiades and Praesepe stellar members, we selected Pleiades members from $K = 11.5$–12, and Praesepe members from K=12–12.5. These two sets of sources should be fully contracted (according to the models), and should represent the $T_{\rm eff} \sim 3500$–3600 K range (since we have corrected for distance). We see no significant difference in the colours, with $J - H = 0.53 \pm 0.03$ and 0.54 ± 0.03, and $H - K = 0.35 \pm 0.03$ and 0.33 ± 0.04 for the Pleiades and Praesepe, respectively. Praesepe is known to be slightly metal-rich compared with the Pleiades, with

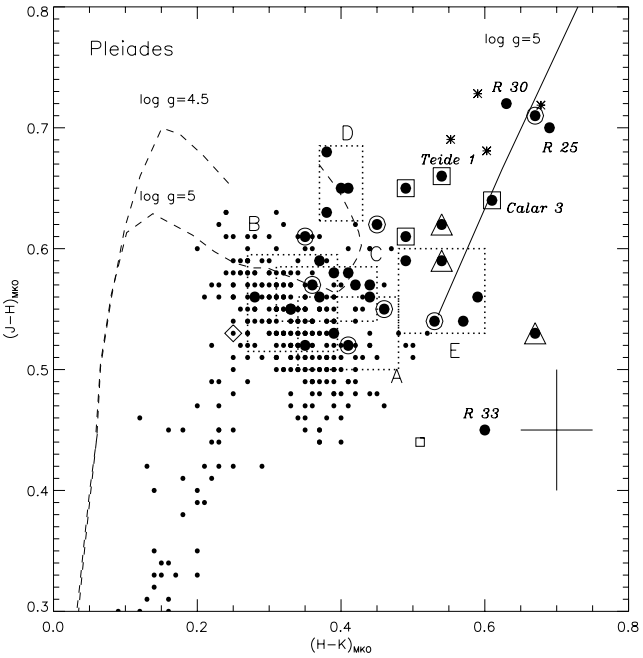

Figure 8. The $J - H$, $H - K$ 2–colour diagram of the Pleiades. Symbols are the same as in Fig. 2. Individual sources are labelled in italic (R = Roque).

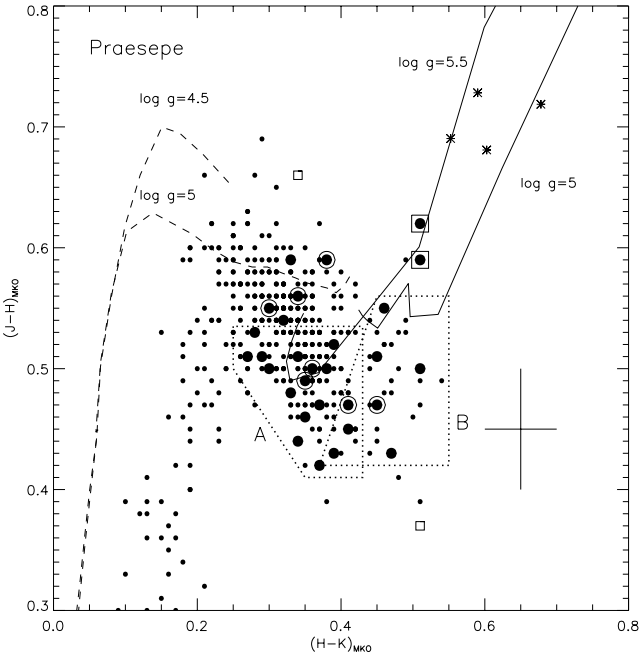

Figure 9. The $J - H$, $H - K$ two-colour diagram of Praesepe. Symbols are the same as in Fig. 2.

[Fe/H] = 0.04 ± 0.04–0.14 (Friel & Boesgaard 1992; Reglero & Fabregat 1991). However, this does not appear to significantly affect the stellar NIR colours, consistent with the model predictions in this $T_{\rm eff}$ range.

In order to show what is happening at cooler $T_{\rm eff}$ values, we grouped the sources into a number of K-magnitude bins. Above the gap we selected Pleiades bins of $K = 13.6$–14.1 and 14.1–14.65, and Praesepe bins of $K = 14.5$–15.3 and 15.3–15.85. We labelled these bins A and B, respectively, and they should correspond to approximately the same $T_{\rm eff}$ ranges in each cluster (∼3150–3000 K for A and 3000–2800 K for B). Below the gap, we considered three additional Pleiades bins. The $K = 14.9$–15.13 range (bin C) contains objects on the flat section of the *IK* CMD (see Section 3.2). The $K = 15.13$–15.5 range (bin D) contains objects at the top of the turn down, where the sequence begins to drop towards the Dusty isochrone in the *IK* CMD. Finally, the $K = 15.5$–16.1 range (bin E) contains objects from near the base of the turn down region, where the *IK* sequence is joining on to the Dusty isochrone. These bins are indicated on the *IK* and *JK* CMDs with dotted lines, and in the *JHK* diagrams by boxes drawn with dotted lines. In the Pleiades, bin A contains 2MASS sources, and we defined the box dimensions using the standard deviation of the average bin colours. For the remaining bins we defined the box dimensions by attempting to include all non-binary member sources within the box dimensions.

When we compare the colour–colour location of bins A and B in each of the clusters, it can be seen that they differ. In the Pleiades, bins A and B have similar colours, and lie very close to the NextGen model predictions for their $T_{\rm eff}$ range. However, in Praesepe these bins have $J - H$ colours that are ∼0.1 bluer than this, and bin B has an $H - K$ colour ∼0.1 redder. The surface gravities expected for these bins are $\log g = 5$ for the Pleiades and $\log g = 5.15$–5.25 for Praesepe, and these differing surface gravities may provide the explanation for the differing colours. We do not expect any atmospheric dust formation for objects in these bins since their $T_{\rm eff}$ values are too high (see Tsuji 2002, fig. 7, and Jones & Tsuji 1997), so gravity-sensitive dust formation cannot provide the explanation. However, molecular opacities (such as H_2O) could be more sensitive to gravity (or pressure) than the NextGen models predict and future generations of models with updated EOS and opacity data may account for these colour changes.

Moving to fainter cooler objects in Praesepe, it can be seen that the faint binary candidate below bin B lies on the dusty isochrone, consistent with dust formation beginning in Praesepe at around $T_{\rm eff} \sim 2500$ K. However, in the Pleiades we are faced with a rather different story. Moving across the gap from bin B to C produces no significant change in colour, and between bins C and D there is then an increase of ∼0.1 in $J - H$. These changes are all consistent with the NextGen isochrone. Pleiades sources eventually move on to the dusty isochrone between bins D and E, and the two faintest Pleiades sources (Roque 25 and 30) both lie on the Dusty isochrones. A possible explanation for these near-infrared colours is that dust does not begin to form in Pleiades sources until $T_{\rm eff} \sim 2000$ K (between bins D and E). This might occur because in lower-gravity atmospheres the lower pressures could suppress dust formation until lower $T_{\rm eff}$s. However, one would also expect that lower gravity atmospheres would be more extended, and have lower outer temperatures, which would have the opposite effect.

Assuming that the differences in colour between Pleiades and Praesepe sources result from differing surface gravities, then one might expect even greater differences for sources found in star-forming regions. This would have implications for the derreddening process that is commonly used for such sources (e.g. Lucas & Roche 2000).

We have flagged likely non-members using the location of bins A to E and the Dusty model atmosphere predictions (for the faintest sources) as a guide. Old disc sources appeared too blue in $J - H$, and several non-stellar sources were also identified amongst our data by their extremely red colours. One object in Fig. 7 (Roque 33) appears to be too blue in $J - H$. This object is a proper motion member, however (see Table A1), and we note that its photometric errors are ∼0.2 in colour, making them not inconsistent with membership. We also used the Pleiades *JHK* diagram to identify some additional unresolved binaries. In the turn down region of both the *IK* and the *JK* CMDs (where the sequence is dropping steeply down towards the Dusty isochrones), there remains some degeneracy between mass and binarity. However, we were able to break this degeneracy using our *JHK* diagram. A single source with $K = 15.13$–15.5 should lie in bin D. However, three sources in this magnitude range lie in (or very near to) bin E. These are presumably near equal-mass binaries, where both components of each binary come from bin E (we refer to them as *JHK* binaries). These binaries are overplotted with an additional open triangle in the figures.

3.6 Summary of membership criteria

Using the *IK* and *JK* CMDs, as well as the *JHK* diagrams, we have assigned photometric membership criteria to our Pleiades and Praesepe samples (see the Appendices). In the Pleiades, we flagged five of the 30 BPL BD candidates as non-members. The remaining 25 BPL candidates, and the nine additional Pleiades candidates from the literature look like cluster BDs. Examination of Table A1 shows that our criteria for these sources are consistent with existing spectroscopic and astrometric measurements, where they exist. It is particularly encouraging that we were able to flag CFHT-PL-18 (BPL 283) as a background binary from its photometry alone. This source was a suspected BD binary, and was only confirmed as a background source when Martín et al. (2000) failed to detect lithium in its spectrum. BPL 45 has been flagged as the same type of object based on its measured J- and K-band photometry alone. Of the Pleiades low-mass star candidates, we flag 14 non-members out of the 194 candidates. This represents only 7 per cent spurious sources in the sample. In Praesepe, we identify higher levels of contamination for our faintest sources. We flag 20 non-members out of the 26 RIZ-Pr candidates, and 37 non-members out of the 89 IZ-Pr candidates. However, for the brighter HSHJ sources we only flag 21 non-members out of 458. The position of Roque-Pr 1 in the *IK* and *JK* CMDs is consistent with membership. However, if it is a member, it must be an unresolved BD binary.

3.7 BD binary mass ratios

Fig. 10 shows two regions of the Pleiades *IK* and *JK* CMDs, focusing on the candidate BDs. The symbols mean the same as in Fig. 2. NextGen and Dusty isochrones are shown with dashed lines, and our cluster sequences (see Sections 3.2 and 3.4) are shown as solid lines. We also show the effects of unresolved binarity, with the use of binary tracks (shown as dotted lines). To construct these binary tracks we started with the single star point which is to form the primary. Then, by combining the magnitude of this primary with that of the faintest point on the sequence (lowest mass), we obtained a new binary point which we joined to our primary point by a dotted line. We then repeated this process for higher mass secondaries, joining

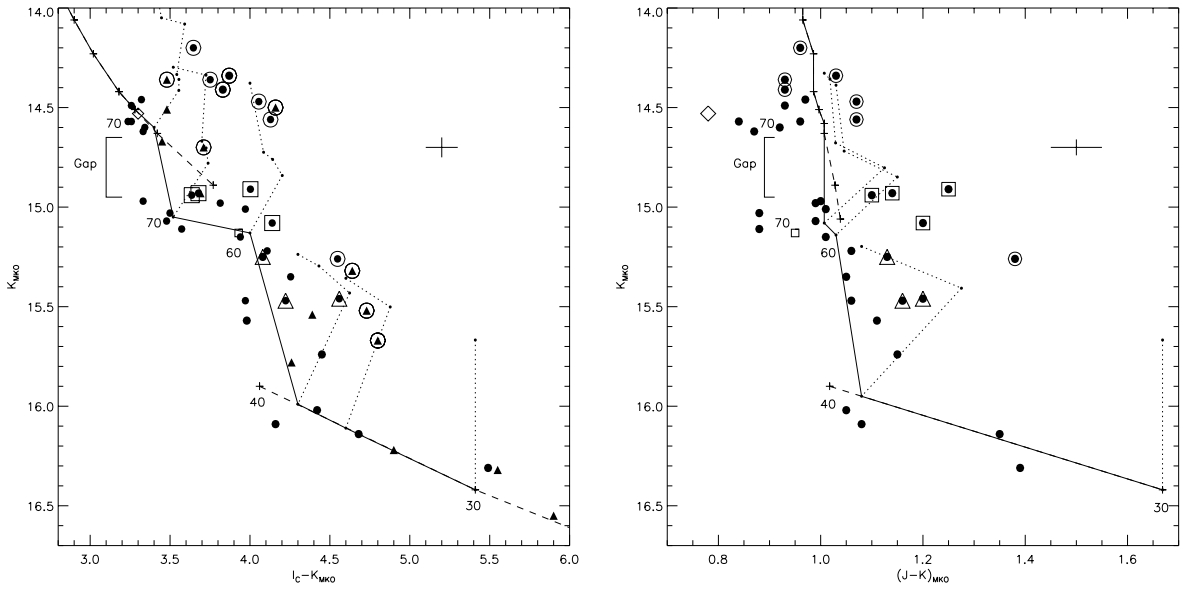

Figure 10. K, $I-K$ and K, $J-K$ CMDs of Pleiades BDs.

each new point to its predecessor until we reach an equal-mass binary, 0.75 mag above the original primary. We also show five mass points on the CMDs (in units of 0.001 $M_\odot$). The 0.07-$M_\odot$ point just above the M dwarf gap is the NextGen model prediction for a 125-Myr isochrone. Since we believe that the M dwarf gap results from a sharp drop in the luminosity–mass relation, we assumed that the mass just below the M dwarf gap is very similar to the mass just above it. Hence, we have a 0.07-$M_\odot$ point just below the M dwarf gap also. The 0.06-$M_\odot$ mass point was estimated from the Pleiades mass–I relation of Dobbie et al. (2002c), which accounts for the M dwarf gap, and was derived using the Pleiades I-band BD LF, and an assumed power-law MF. We note that this agrees with the NextGen and Dusty model J-band predictions, if they are offset by the J magnitude width of the M dwarf gap. The final two mass points are Dusty model predictions for a 125-Myr isochrone. The 0.04-$M_\odot$ mass point should be reasonably representative of the point where the sequence joins the Dusty isochrone. We also note that Dobbie et al. (2002c) suggest that model predictions for the masses of Pleiades BDs from $I = 18.5$–19.5 are too low (by up to 0.01 $M_\odot$), which may have some bearing on the Dusty mass estimates.

When analysing these CMDs, we must consider the depth effect of the cluster. Sources near the front and back of the cluster will appear slightly brighter and fainter, respectively, than they would in the cluster centre. The tidal radius of the Pleiades is 13.1 pc (Pinfield et al. 1998) giving a full depth of ±0.2 mag. However, the majority of sources will be found closer to the cluster centre. Jameson et al. (2002) fit a King profile (King 1962) to the spatial distribution of Pleiades BDs, and derived a core radius of 5 pc. We would expect $\sim$80 per cent of members to lie within this core radius, giving a more likely depth of ±0.1 mag. In order to estimate binary mass ratios (q) for our unresolved binary candidates, we compared their positions with the binary tracks in both CMDs, and estimated q ranges consistent with the photometric errors and the depth effect of the Pleiades. We did this for a depth effect of ±0.1 and ±0.2. We also estimated q ranges on the basis that the Dusty isochrone masses may be higher by 0.01 $M_\odot$. And finally, we made a small allowance for the known (or suspected) variables (PPL1 and Calar 3). Our results are summarized in Table 2. Column 3 indicates whether the source is an *IK*, a *JK* or a *JHK* binary (identified from the *IK* CMD, the *JK* CMD of the *JHK* diagram). Column 4 gives the estimated q range from the mass points in Fig. 9 and a ±0.1 depth effect. Column 5 gives a larger q range, estimated with the full ±0.2 depth effect, and accounting for the uncertainty in the Dusty isochrone mass points (assuming they may be 0.01 $M_\odot$ too low).

Where a source appeared in both CMDs, we found q ranges that were consistent (to within photometric errors) for all but two candidates; CFHT-PL-18 (BPL 283) and BPL 45 appear red in the *JK* CMD, but do not appear sufficiently red in the *IK* CMD. The component sources of these binaries would therefore be too blue in $I-K$ to be cluster members. This is confirmed for CFHT-PL-18, which is a known background binary (see Section 3.4). We have also flagged BPL 45 as a probable non-member, based on its measured photometry alone. CFHT-PL-12 (BPL 294) and INT-PL-IZ-42 could have primaries that are either just above or just below the M dwarf gap. However, CFHT-PL-12 would need to be near the front of the cluster if its primary was from below the gap. Roque 4 lies quite high in the *JK* CMD, suggesting that it may be a foreground object. However, it could still be a binary BD if it is at the front of the cluster, and may alternatively be a BD triple system. We were unable to estimate good q for the two faintest binaries, since we do not know the form of the cluster sequence for masses below 0.03 $M_\odot$.

It is clear that the majority of the unresolved binary candidates have fairly high q values. Indeed, 15 of the 18 probable binary BDs appear to have $q > 0.7$. However, the photometry of three sources is inconsistent with them being either single or $q > 0.7$ binaries. One of these is without J- or H-band measurements, and has not been confirmed as a cluster member (by either a proper motion measurement or the lithium test). The other two are Teide 1 and Calar 3, which are bona fide cluster BDs. We have previously discussed (Section 3.4) other possible causes for the red $J-K$ colours seen in these sources, and concluded that binarity was the most likely cause. We note in addition that the position of these sources in the *JHK* diagram is also consistent with binarity, since they appear partway between bins D/E and the location of Roque 25. These few objects therefore suggest that BD binaries are not all high-q systems. They could consist of two populations; the majority in high-q systems,

Table 2. Pleiades BD binary mass ratios (q). The q_1 ranges were estimated assuming a depth effect of ± 0.1 mag, and masses from Fig. 9. q_2 ranges were estimated assuming a depth effect of ± 0.2 mag, and accounting for the fact that the Dusty isochrone masses could be underestimated by ~ 0.01 $M_\odot$.

Binaries	Other names	Binary type	q_1	q_2	Notes
BPL 45		*JK*			Probable BG source
BPL 66	Roque 4	*IK*		~ 1	Near front of cluster?/Triple BD?
BPL 79	Roque 13	*IK*	0.7–1	0.65–1	
BPL 108	Roque 14	*IK*	0.8–1	0.75–1	
BPL 137	Teide 1	*JK*	0.55–0.65	0.5–0.9	
BPL 142	Roque 17	*IK*	0.7–1	0.65–1	
BPL 235	Calar 3	*JK*	~ 0.5	0.5–0.7	
BPL 249		*JHK*	~ 1		
BPL 283	CFHT-PL-18	*JK*			Known BG source
BPL 294	CFHT-PL-12	*IK*	0.6–0.9	0.4–1	Primary probably above gap
BPL 303	CFHT-PL-25	*JHK*	<0.75	<1	
PPL 1	Roque 15	*IK*	0.8–1	0.75–1	
PPL 15	IPMBD 23, NPL35	*IK*	0.7–1	0.65–1	Known binary with $q = 0.85$
CFHT-PL-16		*IK*	0.8–1	0.75–1	
CFHT-PL-23		*JHK*	~ 1		
INT-PL-IZ-20		*IK*		<0.8	
INT-PL-IZ-25		*IK*	~ 0.8		
INT-PL-IZ-42		*IK*	0.4–0.6 or ~ 1	0–0.7 or ~ 1	Primary above or below gap?
INT-PL-IZ-43		*IK*	0.4–0.65	0–0.8	
INT-PL-IZ-76		*IK*	0.9–1	0.8–1	

and a smaller fraction in low-q systems. Theoretical simulations are not yet at a level to make such predictions. However, the hydrodynamical simulation of Bate, Bonnell & Bromm (2002) shows BDs forming from the collapse and fragmentation of a turbulent molecular cloud. They determined that ~ 75 per cent of BDs form by the fragmentation of gravitationally unstable circumstellar discs, with subsequent ejection removing the BD from the region of dense gas. The remaining 25 per cent were found to form from the fragmentation of dynamically collapsing filamentary gas, where the forming BDs fell into, and were rapidly ejected from unstable multiple systems (see also Reipurth & Clarke 2001). However, this simulation only produced one BD binary, but lacked the spatial resolution to predict very close systems. Future simulations with higher spatial resolution may reveal a link between the two different formation mechanisms and the resulting q distribution of BD binaries.

3.8 Binary fractions

We determined binary fractions (BF; defined as the number of binary systems in some photometric range divided by the total number of systems in that range) using the *IK* CMDs in general, for a number of photometric ranges. The results are given in Table 3, where the uncertainties are determined assuming binomial statistics (see Burgasser et al. 2003). The mass ranges were estimated using our *IK* cluster sequences (see Section 3.2). The stellar q ranges were estimated by simulating the effect of unresolved binarity in the *IK* CMDs (as was done in Section 3.7 for the Pleiades BDs), and finding the q value when the binary track crosses midway between the single star sequence and the binary sequence 0.75 mag above it.

Starting in Praesepe, the first range we considered was from $I - K = 1$–1.9 (G and K stars). The single stars all bunch around the predicted sequence, and we flagged binaries by their proximity to the binary star sequence. The next range we chose was from $I - K = 1.9$–2.5 (where the upper limit represents the completeness of 2MASS and the HSHJ survey). The sources lie in a fairly straight path down the CMD in this range, and we therefore chose to separate binaries and single stars using a straight line. We defined this separation line such that the average spread of members above and below it was the same (as one would expect for a binary-induced spread). And by doing this for two subranges ($I - K = 1.9$–2.2 and 2.2–2.5) we ensured that the gradient of the line was correct. We would expect a spread of ± 0.375 to represent the full spread induced from binarity, and we obtained spreads of ± 0.36 and ± 0.43 for the two ranges, respectively. The slightly larger value for the redder range

Table 3. Binary fractions for the Praesepe and Pleiades samples. Spectral types were estimated using Leggett (1992).

Praesepe $I - K$	Mass/SpT	q-sensitivity	Binary fraction
1–1.9	1.0–0.6 $M_\odot$ G/K stars	0.5–1	17^{+6}_{-4} per cent
1.9–2.5	0.6–$\sim$0.2 $M_\odot$ M0–M5	0.35–1	41 ± 5 per cent
1.9–2.2	0.6–$\sim$0.35 $M_\odot$ M0–M3	0.3–1	31^{+7}_{-6} per cent
2.2–2.5	$\sim$0.35–$\sim$0.2 $M_\odot$ M3–M5	0.4–1	44 ± 6 per cent
3–3.6	$\sim$0.11–$\sim$0.09 $M_\odot$ M6–M7	0.65–1	47^{+13}_{-11} per cent
Pleiades			
1–1.9	1.0–0.6 $M_\odot$ G/K stars	0.5–1	23^{+6}_{-5} per cent
2.6–3	0.15–0.09 $M_\odot$ M5–M6	$\sim$0.35–1	36 ± 5 per cent
2.6–2.8	0.15–0.11 $M_\odot$ M5	0.35–1	27^{+6}_{-5} per cent
2.8–3	0.11–0.09 $M_\odot$ M6	0.4–1	51 ± 8 per cent
3.3–4.3	0.07–0.05 $M_\odot$ M7–M8	0.5–1	50^{+11}_{-10} per cent

is accounted for by larger photometric errors. This approach has the added benefit that it is independent of any assumed distance modulus. Table 3 gives the binary fraction for both subranges, as well as for the full range. For the lowest-mass Praesepe stars we chose to use $I - K = 3$–3.6 (where we just have UKIRT photometry). This avoids the CMD overlap region between the photographic and CCD surveys, where different survey areas and photometric errors complicate matters. Binaries in this range were flagged in Section 3.2. Unlike the higher-mass ranges, these candidates do not have proper motions. However, using the disc luminosity function of Kirkpatrick et al. (1994), we expect no more than ∼1 and ∼0.5 field star to contaminate the single and binary star sequences, respectively. Such numbers will not significantly affect our statistics.

For the Pleiades, the first range we considered was from $I - K =$ 2.6–3. We took the same approach as for Praesepe, and divided this range in two ($I - K = 2.6$–2.8 and 2.8–3), defining a selection line such that the scatter above and below (in each region) was identical. The spread about the selection line was ±0.57 for each of the subregions. This is somewhat more than the expected ±0.375, but the additional spread will be predominantly due to photometric errors and cluster depth. Finally, we considered a BD range. We counted single BDs below the M dwarf gap that have $K < 15.5$, since our sample is spatially complete in this range. The mass range for the single stars is ∼0.07–0.05 $M_\odot$, where we have interpolated between the 0.06 and the 0.04 $M_\odot$ points in Fig. 9. We then counted binary BDs that could have primaries amongst these single sources, including objects from $K = 14.2$–15.2. We note that we ignored CFHT-PL-12 (BPL 294) since it is likely that its primary comes from above the gap. In this way, we selected 10 single BDs and 10 binary BDs. We estimated the q sensitivity range for our BD binaries using Table 2.

We have already discussed how the cluster depth affects BD binaries. However, it will also be a source of error for our stellar BFs. Objects with a position on the CMD that is within the cluster depth (e.g. 0.2 and 0.15 mag for the Pleiades and Praesepe, respectively) of the binary selection line could potentially spill over this line if they were near the front or the back of the cluster. This represents 53 per cent of Pleiades sources and 40 per cent of Praesepe sources. However, the cluster spatial distributions (Pinfield et al. 1998; Holland et al. 2000) indicate that of these stars, we would only expect ∼5–15 and ∼5–10 per cent of Pleiades and Praesepe stars, respectively, to actually spill across the line. Furthermore, an error will only occur if the BF itself is different from 50 per cent (for BF = 50 per cent misidentified binaries and single stars will cancel out). Combining these together, we would expect no more than ∼1 and 2 per cent BF errors in Praesepe and the Pleiades, respectively, due to depth effects.

Another source of error comes from variability, resulting from chromospheric activity such as spots or flares pushing some single stars intermittently above the binary selection line. Lockwood et al. (1984) found that ∼40 per cent of Hyades F G and K dwarfs varied at a level of ∼1–2 per cent. For later types, Stauffer et al. (1991) reported Hα emission in ∼60 per cent of late K–mid M Hyades members, as well as in the vast majority of G–mid M Pleiades members, and Scholz, Eisloffel & Mundt (2000) found photometric variations among young M dwarfs similar to those of solar type stars. Therefore, although many of our members may be variable, we expect this variability to be generally low (a few per cent). More violent flares are occasionally seen in late M dwarfs (Liebert et al. 1999), but are rare. We estimate that our stellar BF values should not be increased by more than ∼5 per cent as a result of variability.

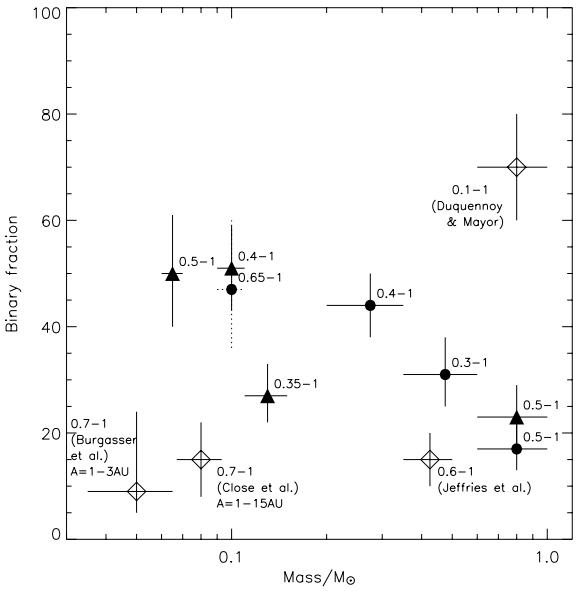

Figure 11. The binary fractions of the Pleiades (triangles) and Praesepe (circles). Four points from the literature are shown as open diamonds. At 0.1 $M_\odot$ the BF error bars of two points overlap, so we plot the Praesepe error bars as a dotted line for clarity. The q ranges are indicated next to each point, as is an A range for each of the Burgasser and Close points.

The BF values are plotted in Fig. 11, as a function of mass. Filled triangles and circles represent Pleiades and Praesepe data, respectively. Additional points from the literature are shown as open diamonds. The highest-mass point agrees well with the field star results of Duquennoy & Mayor (1991), which increases to 70 per cent for $q = 0.1$–1. From 0.6–0.35 $M_\odot$ we find a BF of ∼30 per cent. The BF of NGC 2516 agrees with this value for ∼0.6 $M_\odot$, but drops to ∼15 per cent for 0.5–0.35 $M_\odot$ (Jeffries, Thurston & Hambly 2001). This difference could be explained by the fact that the NGC 2516 CMD was only sensitive to $q = 0.6$–1 binaries, whereas our CMD is sensitive to $q = 0.3$–1. If the clusters have intrinsically similar binary populations, then this implies that there is a BF of 15 per cent from $q = 0.3$–0.6 as well as from $q = 0.6$–1, suggesting a flat BF–q distribution in this mass range. This represents a departure from the BF–q distribution of solar-type field stars, which rises towards lower q. If the BF–q distribution were like that of solar-type stars we would expect a BF of 30 per cent for $q = 0.3$–0.6, and thus 45 per cent for $q = 0.3$–1. Our result is 1.5σ lower than this value. A flat binary–q distribution would give a total BF of ∼45 per cent in this mass range. Next, with the exception of the Pleiades point at 0.13 $M_\odot$, there is a general trend of increasing BF towards lower mass. The q ranges of these points are fairly similar, and so should not significantly bias this trend. Moving into the substellar regime, it can be seen that the BD binary fraction is around 50 per cent. Even if we are extremely conservative, and only select the most obvious BD binaries from the *IK* CMD (assuming that *JK* and *JHK* binaries are, in fact, single), we find a BF of 32^{+11}_{-8} per cent. Fig. 11 also shows the T dwarf BF resolved by the *HST* (Burgasser et al. 2003), and the late M/early L dwarf BF resolved by Hokupa'a on Gemini (Close et al. 2003). Mass range estimates were taken from Close et al. (2003), and estimated for the T dwarfs assuming an age range of 1-5Gyrs. Both these BFs (9^{+15}_{-4} and 15 ± 7 per cent, respectively) are significantly lower than our BF for Pleiades BDs. However, these observations were only sensitive to binaries with separations >1 au. It is possible that the total BF of these populations is

identical to that of Pleiades BDs if 70–80 per cent of BD binaries have separations <1 au. It may be that many BD binaries are like PPL15 (Basri & Martín 1999) which has a separation of 0.03 au. We also note that the *N*-body simulations of Kroupa (2001) and Kroupa, Aarseth & Hurley (2001) suggest that $\sim$50 per cent of cluster BD binaries with $\log P/d = 1$–6 (separations of $\sim$0.04–90 au) would be disrupted during the first few Myr of protocluster dynamical evolution. This would require an even higher initial BD BF, unless most BD binaries are extremely tight. However, the hydrodynamical simulation of Bate, Bonnell & Bromm (2002) predicts an initial BF of $\sim$5 per cent, since only 1 BD binary was produced in their simulation among 20 single BDs. But the spatial resolution of this simulation was not high enough to model the formation of extremely close BD binaries. Such binaries may form during a secondary collapse phase of individual pressure supported fragments (Bonnell & Bate 1994). If this is not the case (Bate 1998), then post-fragmentation processes (such as dynamical interactions) might be responsible for creating extremely tight BD binaries (by hardening).

4 FUTURE WORK

Proper motion measurements have already been made for 15 of the BD candidates discussed here. Work is currently underway by some of us to measure proper motions of the remaining Pleiades BDs. It will be particularly useful to confirm all possible low-q BD binaries as Pleiades members. Measuring proper motions of the Praesepe candidates is also important, and is in progress (Chappelle, Pinfield & Steele 2002). Such measurements will allow us to define the Praesepe cluster sequence with more confidence. Also, the faintest Praesepe candidates could be BDs, and would be the first identified in an intermediate age cluster.

Measuring NIR spectra is a natural next step if we are to understand the nature of the cluster sequences. These spectra could be compared with the predictions of both NextGen and Dusty model atmospheres, to determine when dust is beginning to form in the atmospheres of Pleiades and Praesepe sources, and what effects it has in the different surface gravities. Furthermore, the best way to improve on our analysis of binarity is from NIR spectra. We could combine the spectra of likely single sources, and compare the results with spectra of suspected unresolved binaries, to confirm whether or not these sources really are binary in nature.

The nature of the M dwarf gap could be further investigated by measuring longer-wavelength photometry (e.g. L band) of sources on either side of the M dwarf gap, to look for evidence (or lack of it) of dust formation.

Deeper and larger-scale surveys of the clusters will provide much larger samples of members to work with. The 16 deg^2 survey recently obtained as part of the WFS with the INT and WFC should identify several hundred Pleiades BDs. Also, the WFC survey of Praesepe made by Chappelle et al. (2002) should identify large numbers of very low-mass stars and possibly BDs. With these larger samples we will be able to more accurately measure the M dwarf gap in both clusters, as well as to obtain a better statistical measure of the BD binary fraction and binary-q distribution.

ACKNOWLEDGMENTS

DJP and PDD acknowledge funding from PPARC. AK acknowledges funding from the Leverhulme Trust. The United Kingdom Infrared Telescope is operated by the Joint Astronomy Centre on behalf of the UK Particle Physics and Astronomy Research Council. Some of the data reported here were obtained as part of the UKIRT Service Programme. This publication makes use of data products from the Two Micron All-sky Survey, which is a joint project of the University of Massachusetts and the Infrared Processing and Analysis Centre/California Institute of Technology, funded by the Aeronautics and Space Administration and the National Science Foundation.

REFERENCES

Allard F., Hauschildt P.H., Alexander D.R., Starrfield S., 1997, ARA&A, 35, 137
Allard F., Hauschildt P.H., Alexander D.R., Tamanai A., Schweitzer A., 2001, ApJ, 556, 357
Bailer-Jones C.A.L., Mundt R., 2001, A&A, 367, 218
Baraffe I., Chabrier G., Allard F., Hauschildt P.H., 1998, A&A, 337, 403
Barrado y Navascués D., Bouvier J., Stauffer J.R., Lodieu N., McCaughrean M.J., 2002, A&A, 395, 813
Basri G., Martín E.L., 1999, AJ, 118, 2460
Bate M.R., 1998, ApJ, 508, L95
Bate M.R., Bonnell I.A., Bromm V., 2002, MNRAS, 332, 65
Bessell M.S., 1986, PASP, 98, 1303
Bonnell I.A., Bate M.R., 1994, MNRAS, 271, 999
Bouvier J., Stauffer J.R., Martín E.L., Barrado y Navascues D., Wallace B., Bejar V.J.S., 1998, A&A, 336, 490
Burgasser A.J., Kirkpatrick J.D., Reid I.N., Brown M.E., Miskey C.L., Gizis J.E., 2003, ApJ, 586, 512
Burrows A., Hubbard W.B., Saumon D., Lunine J.I., 1993, ApJ, 406, 158
Burrows A. et al., 1997, ApJ, 491, 856
Carpenter J.M., 2001, AJ, 121, 2851
Chabrier G., Baraffe I., 1997, A&A, 327, 1039
Chabrier G., Baraffe I., Allard F., Hauschildt P.H., 2000, ApJ, 542, 464
Chappelle R.J., Pinfield D.J., Steele I.A., 2002, in Martin E., Proc. IAU Symp. 211, Brown Dwarfs. Astron. Soc. Pac., San Francisco, in press
Close L. M., Siegler N., Freed M., Biller B., 2003, ApJ, 587, 407
Crawford D.L., Perry C.L., 1976, AJ, 81, 419
Dahn C.C. et al., 2002, AJ, 124, 1170
D'Antona F., Mazzitelli I., 1994, ApJS, 90, 467
Dobbie P.D., Kenyon F., Jameson R.F., Hodgkin S.T., 2002a, MNRAS, 331, 445
Dobbie P.D., Kenyon F., Jameson R.F., Hodgkin S.T., Pinfield D.J., Osbourne S.L., 2002b, MNRAS, 335, 687
Dobbie P.D., Pinfield D.J., Jameson R.F., Hodgkin S.T., 2002c, MNRAS, 335, 79L
Duquennoy A., Mayor M., 1991, A&A, 248, 485
Friel E.D., Boesgaard A.M., 1992, ApJ, 387, 170
Hambly N.C., Hawkins M.R.S., Jameson R.F., 1993, A&AS, 100, 607 (HHJ)
Hambly N.C., Steele I.A., Hawkins M.R.S., Jameson R.F., 1995a, A&AS, 109, 29 (HSHJ)
Hambly N.C., Steele I.A., Hawkins M.R.S., Jameson R.F., 1995b, MNRAS, 273, 505
Hauschildt P.H., Allard F., Baron E., 1999, ApJ, 512, 377
Hawarden T.G., Leggett S.K., Letawsky M.B., Ballantyne D.R., Casali M.M., 2001, MNRAS, 325, 563
Hawley S.L., Tourtellot J.G., Reid I.N., 1999, AJ, 117, 1341
Hodgkin S.T., Pinfield D.J., Jameson R.F., Steele I.A., Cossburn M.R., Hambly N.C., 1999, MNRAS, 310, 87
Holland K., Jameson R.F., Hodgkin S.T., Davies M.B., Pinfield D.J., 2000, MNRAS, 319, 956
Jameson R.F., Dobbie P.D., Hodgkin S.T., Pinfield D.J., 2002, MNRAS, 335, 853
Jeffries R.D., Thurston M.R., Hambly N.C., 2001, A&A, 375, 863
Jones H.R.A., Tsuji T., 1997, ApJ, 480, L39
King I.R., 1962, AJ, 67, 471
Kirkpatrick J.D., Henry T.J., McCarthy D.W., Jr, 1991, ApJS, 77, 417
Kirkpatrick J.D., McGraw J.T., Hess T.R., Liebert J., McCarthy D.W., Jr, 1994, ApJS, 94, 749
Kirkpatrick J.D., Henry T.J., Simons D.A., 1995, AJ, 109, 797

Kroupa P., 2001, MNRAS, 322, 231
Kroupa P., Tout C.A., Gilmore G., 1990, MNRAS, 244, 76
Kroupa P., Aarseth S., Hurley J., 2001, MNRAS, 321, 699
Leggett S.K., 1992, ApJS, 82, 351
Leggett S.K., Allard F., Hauschildt P.H., 1998, ApJ, 509, 836
Liebert J., Kirkpatrick J.D., Reid I.N., Fisher M.D., 1999, ApJ, 519, 345
Lockwood G.W., Thompson D.T., Radick R.R., Osborn W.H., Baggett W.E., Duncan D.K., Hartmann L.W., 1984, PASP, 96, 714
Lucas P.W., Roche P.F., 2000, MNRAS, 314, 858
Lynga G., 1987, Catalogue, 5th edn, Strasbourg
Magazzu A., Rebolo R., Zapatero-Osorio M.R., Martín E.L., Hodgkin S.T., 1998, ApJ, 497, 47
Makarov V.V., 2002, AJ, 124, 3299
Martín E.L., Kun M., 1996, A&AS, 116, 467
Martín E.L., Rebolo R., Zapatero-Osorio M.R., 1996, ApJ, 469, 706
Martín E.L. et al., 1998, ApJ, 509, 113
Martín E.L., Delfosse X., Basri G., Goldman B., Forveille T., Zapatero-Osorio M.R., 1999, AJ, 118, 2466
Martín E.L., Brandner W., Bouvier J., Luhman K.L., Stauffer J., Basri G., Zapatero-Osorio M.R., Barrado y Navascues D., 2000, ApJ, 543, 299
Mermilliod J.-C., Turon C., Robichon N., Arenou F., Lebreton Y., 1997, in Proc. ESA Symp. 'Hipparcos – Venice '97', 643
Moraux E., Bouvier J., Stauffer J.R., 2001, A&A, 367, 211
Nissen P.E., 1988, A&A, 199, 146
Pinfield D.J., 1997, PhD thesis, Univ. Leicester
Pinfield D.J., Hodgkin S.T., Jameson R.F., Cossburn M.R., von Hippel T., 1997, MNRAS, 287, 180
Pinfield D.J., Jameson R.F., Hodgkin S.T., 1998, MNRAS, 299, 955
Pinfield D.J., Hodgkin S.T., Jameson R.F., Cossburn M.R., Hambly N.C., Devereux N., 2000, MNRAS, 313, 347 (BPL)
Prosser C.F., 1992, AJ, 103, 488
Rebolo R., Martín E.L., Basri G., Marcy G.W., Zapatero-Ozorio M.R., 1996, ApJ, 469, L53
Reglero V., Fabregat J., 1991, A&AS, 90, 25
Reid I.N., Cruz K.L., 2002, AJ, 123, 2806
Reipurth B., Clarke C., 2001, AJ, 122, 432
Scholz A., Eisloffel J., Mundt R., 2000, Astron. Ges. Abs. Ser., 17, A05
Scrutskie M.F. et al., 1995, 187, 7507
Sharp C.M., Huebner W.F., 1990, ApJS, 72, 417
Simons D.A., Tokunaga A., 2002, PASP, 114, 169
Stauffer J.R., Giampapa M.S., Herbst W., Vincent J.M., Hartmann L.W., Stern R.A., 1991, ApJ, 374, 142
Stauffer J.R., Schultz G., Kirkpatrick J.D., 1998, ApJ, 499, L199
Stauffer J.R. et al., 1999, ApJ, 527, 219
Tsuji T., 2002, ApJ, 575, 264
van Leeuwen F., 1999, A&A, 341, 71L
Zapatero-Ozorio M.R., Rebolo R., Martín E.L., Basri G., Magazzu A., Hodgkin S.T., Jameson R.F., Cossburn M.R., 1997, ApJ, 491, L81
Zapatero-Osorio M.R., Rebolo R., Martín E.L., Hodgkin S.T., Cossburn M.R., Magazzu A., Steele I.A., Jameson R.F., 1999, A&AS, 134, 537

APPENDIX A: TABLES OF PHOTOMETRY

Table A1. Photometry (c3–6), membership criteria (c7–9, c11–13) and binarity (c10) of Pleiades BD candidates. Membership is from the *IK* CMD, the *JK* CMD and the *JHK* diagram. Refs; (a) Martín, Rebola & Zapatero-Ozorio (1996), (b) Rebolo et al. (1996), (c) Zapatero-Osorio et al. (1997), (d) Martín et al. (1998) (e) Stauffer, Schultz & Kirkpatrick (1998), (f) Martín et al. (2000), (g) Pinfield et al. (2000), (h) Moraux, Bouvier & Stauffer (2001), (i) Jameson et al. (2002), (j) Dobbie (2002) private communication. A ⋆ indicates a non-member by virtue of binarity.

Name	Other names	I_C	J_{MKO}	H_{MKO}	K_{MKO}	*IK*	*JK*	*JHK*	Bin	SpT	pm	Li
BPL 45		18.61[g]	16.07 ± 0.05	15.42 ± 0.03	14.93 ± 0.04	y	N⋆	y	b	y		
BPL 49	CFHT-Pl-17	18.55[g]	16.12 ± 0.04[g]	15.49 ± 0.07[g]	15.07 ± 0.06[g]	y	y	y			y[h]	
			16.14 ± 0.10[i]	15.51 ± 0.11[i]								
			15.99 ± 0.04	15.48 ± 0.05								
BPL 62	Roque 7	19.44[g]	16.53 ± 0.03[g]	15.85 ± 0.02[g]	15.47 ± 0.02[g]	y	y	y			y[h]	
	CFHT-Pl-24		16.55 ± 0.18[i]	15.88 ± 0.14[i]								
BPL 66	Roque 4	19.81[g]	16.66 ± 0.05	15.93 ± 0.03	15.26 ± 0.04	y	y	y	b	y[c]		
			16.62 ± 0.04	15.92 ± 0.05	15.26 ± 0.04							
			16.69 ± 0.12[i]	16.04 ± 0.09[i]								
BPL 76		17.83[g]	15.41 ± 0.04	14.85 ± 0.03	14.57 ± 0.06[g]	y	y	y				
BPL 78		18.98[g]	16.02 ± 0.05	15.45 ± 0.03	15.01 ± 0.04	y	y	y				
BPL 79	Roque 13	18.69[g]	15.63 ± 0.03[g]	15.09 ± 0.02[g]	14.56 ± 0.03[g]	y	y	y	b	y[c]		
			15.65 ± 0.09[i]	15.11 ± 0.08[i]								
BPL 81		18.79[g]	15.97 ± 0.03	15.39 ± 0.05	14.98 ± 0.02[g]	y	y	y				
BPL 100	Roque 9	19.33[g]	16.28 ± 0.03	15.63 ± 0.05	15.22 ± 0.02[g]	y	y	y				
			16.30 ± 0.19[i]	15.72 ± 0.15[i]								
BPL 108	Roque 14	18.53[g]	15.50 ± 0.02[g]	14.89 ± 0.02[g]	14.47 ± 0.03[g]	y	y	y	b	y[c]		
			15.53 ± 0.10[i]	14.96 ± 0.09[i]								
			15.59 ± 0.03	14.96 ± 0.03								
BPL 124		17.78[g]	15.43 ± 0.05	14.85 ± 0.03	14.46 ± 0.04	y	y	y			y[g]	
BPL 132	Roque 11	19.06[g]	16.08 ± 0.03[g]	15.64 ± 0.03[g]	15.13 ± 0.04[g]	y	y	N		y[b]		
	NPL 37											
BPL 137	Teide 1	19.22[g]	16.32 ± 0.05[g]	15.62 ± 0.05[g]	15.08 ± 0.05[g]	y	y	y	b	y[b]	y[h]	y[b]
	NPL 39		16.19 ± 0.11[i]	15.65 ± 0.09[i]								
			16.24 ± 0.05	15.62 ± 0.05								
BPL 142	Roque 17	18.11[g]	15.29 ± 0.03[g]	14.77 ± 0.03[g]	14.36 ± 0.05[g]	y	y	y	b	y[c]	y[g]	
			15.31 ± 0.09[i]	14.79 ± 0.07[i]								
BPL 152	Roque 16	17.95[g]	15.49 ± 0.03[g]	14.97 ± 0.02[g]	14.62 ± 0.03[g]	y	y	y		y[c]	y[h]	y[e]
	CFHT-Pl-11		15.51 ± 0.11[i]	14.99 ± 0.09[i]								
BPL 163		17.83[g]	15.31 ± 0.03	14.78 ± 0.05	14.53 ± 0.04[g]	y	N	y				
BPL 168		17.65[g]	–	–	16.02 ± 0.10	N	–	–				

Table A1 *– continued*

Name	Other names	I_C	J_{MKO}	H_{MKO}	K_{MKO}	*IK*	*JK*	*JHK*	Bin	SpT	pm	Li
BPL 172	Roque 12	18.53[g]	15.91 ± 0.03	15.36 ± 0.05	15.10 ± 0.03[g]	y	y	y		y[c]		
	NPL 36		15.93 ± 0.10[i]	15.44 ± 0.08[i]	14.97 ± 0.07[i]							
BPL 201		19.60[g]	16.40 ± 0.03[g]	15.75 ± 0.03[g]	15.35 ± 0.04[g]	y	y	y				
BPL 202	CFHT-Pl-9	17.75[g]	15.44 ± 0.03	14.88 ± 0.05	14.49 ± 0.04[g]	y	y	y		y[e]	y[h]	N[e]
			15.40 ± 0.04	14.84 ± 0.02								
BPL 235	Calar 3	18.91[g]	16.24 ± 0.03[g]	15.53 ± 0.03[g]	14.91 ± 0.03[g]	y	y	y	b	y[a]	y[h]	y[b]
	CFHT-Pl-21		16.09 ± 0.04	15.49 ± 0.05								
BPL 240		18.68[g]	15.99 ± 0.03	15.44 ± 0.05	15.11 ± 0.03[g]	y	y	y				
BPL 249		20.02[g]	16.66 ± 0.03[g]	16.13 ± 0.03[g]	15.46 ± 0.03[g]	y	y	y	b			
BPL 254	Teide 2	17.81[g]	15.53 ± 0.04	14.94 ± 0.03	14.57 ± 0.06[g]	y	y	y		y[d]	y[h]	y[d,e]
	CFHT-Pl-13		15.53 ± 0.08[i]	14.97 ± 0.07[i]	14.54 ± 0.06[i]							
BPL 283	CFHT-Pl-18	18.58[g]	16.04 ± 0.03[g]	15.43 ± 0.02[g]	14.94 ± 0.06[g]	y	N[⋆]	y	b	y[f]	N[h]	N[f]
BPL 294	CFHT-Pl-12	17.85[g]	15.16 ± 0.03	14.55 ± 0.02	14.20 ± 0.02[g]	y	y	y	b	y[e]	y[h]	y[e]
BPL 303	CFHT-Pl-25	19.69[g]	16.63 ± 0.04	16.01 ± 0.02	15.47 ± 0.06[g]	y	y	y	b		y[h]	
			16.64 ± 0.15[i]	16.05 ± 0.13[i]								
BPL 306		19.09[g]	16.16 ± 0.04	15.53 ± 0.02	15.15 ± 0.02[g]	y	y	y				
BPL 316		18.30[g]	15.97 ± 0.04	15.41 ± 0.02	15.01 ± 0.03	y	y	y				
					14.93 ± 0.04							
BPL 327	IPMBD 11	17.94[g]	15.52 ± 0.03	14.99 ± 0.02	14.60 ± 0.02[g]	y	y	y		y	y[g]	
PPL 1	Roque 15	18.21[i]	15.37 ± 0.08[i]	14.82 ± 0.06[i]	14.34 ± 0.05[i]	y	y	y	b	y		y
PPL 15	IPMBD 23	18.24[i]	15.34[i]	14.77[i]	14.41[i]	y	y	y	b	y	y	y
	NPL 35											
CFHT-PL-23		19.33[i]	16.38 ± 0.08[i]	15.79 ± 0.08[i]	15.25 ± 0.05[i]	y	y	y	b			
Roque 5		20.19[i]	16.89 ± 0.14[i]	16.33 ± 0.15[i]	15.74 ± 0.10[i]	y	y	y				
Roque 8		19.55[i]	16.68 ± 0.11[i]	16.14 ± 0.10[i]	15.57 ± 0.06[i]	y	y	y				
Roque 25		21.80[i]	17.7 ± 0.3[i]	17.0 ± 0.3[i]	16.31 ± 0.19[i]	y	y	y		y		
Roque 30		20.82[i]	17.49 ± 0.12[i]	16.77 ± 0.11[i]	16.14 ± 0.07[i]	y	y	y				
Roque 33	NPL 40	20.44[i]	17.07 ± 0.12[i]	16.62 ± 0.18[i]	16.02 ± 0.08[i]	y	y	?		y	y[j]	y
Roque 36		20.25[i]	17.17 ± 0.20[i]	16.58 ± 0.12[i]	16.09 ± 0.08[i]	y	y	y				

Table A2. Photometry (c2–5) and membership (c6–8) of Pleiades low-mass star candidates (higher mass BPL candidates). Membership is from the *IK* CMD, the *JK* CMD and the *JHK* diagram. $J-H$- and K-band photometry is from 2MASS, and has been transformed into the MKO system.

BPL	I_C	J_{MKO}	H_{MKO}	K_{MKO}	*IK*	*JK*	*JHK*
3	14.81	13.25 ± 0.03	12.74 ± 0.03	12.36 ± 0.03	y	y	y
4	14.17	12.67 ± 0.03	12.12 ± 0.02	11.77 ± 0.03	y	y	y
5	14.25	12.66 ± 0.03	12.17 ± 0.03	11.80 ± 0.03	y	y	y
6	15.74	14.01 ± 0.03	13.53 ± 0.03	13.09 ± 0.04	y	y	y
7	16.28	14.44 ± 0.03	13.92 ± 0.03	13.48 ± 0.04	y	y	y
16	17.02	15.20 ± 0.04	14.67 ± 0.05	14.24 ± 0.06	N	y	y
18	14.39	12.89 ± 0.03	12.35 ± 0.03	11.97 ± 0.03	y	y	y
19	16.39	14.60 ± 0.03	14.09 ± 0.04	13.76 ± 0.04	y	y	y
20	14.81	13.21 ± 0.03	12.70 ± 0.03	12.28 ± 0.03	y	y	y
26	17.00	14.67 ± 0.03	14.16 ± 0.04	13.76 ± 0.05	y	y	y
30	15.90	14.15 ± 0.03	13.58 ± 0.03	13.22 ± 0.04	y	y	y
34	13.72	12.01 ± 0.02	11.45 ± 0.03	11.10 ± 0.03	y	y	y
38	16.12	14.27 ± 0.03	13.78 ± 0.04	13.42 ± 0.04	y	y	y
43	15.81	14.11 ± 0.03	13.56 ± 0.03	13.18 ± 0.04	y	y	y
44	16.09	14.30 ± 0.03	13.76 ± 0.03	13.37 ± 0.04	y	y	y
56	14.90	13.29 ± 0.03	12.74 ± 0.02	12.40 ± 0.03	y	y	y
58	17.69	15.37 ± 0.05	14.77 ± 0.06	14.23 ± 0.07	y	y	y
61	14.86	13.11 ± 0.02	12.58 ± 0.03	12.23 ± 0.03	y	y	y
68	14.33	12.85 ± 0.03	12.34 ± 0.03	12.03 ± 0.04	y	y	y
69	17.59	16.61 ± 0.15	16.10 ± 0.20	15.56 ± 0.18	N	y	y
70	15.40	13.33 ± 0.02	12.76 ± 0.03	12.45 ± 0.03	y	y	y
71	15.14	13.18 ± 0.02	12.58 ± 0.03	12.23 ± 0.03	y	y	y
72	16.18	14.04 ± 0.03	13.52 ± 0.03	13.20 ± 0.03	y	y	y
73	15.09	13.08 ± 0.02	12.60 ± 0.03	12.21 ± 0.03	y	y	y
74	17.44	15.19 ± 0.05	14.68 ± 0.06	14.23 ± 0.06	y	y	y
75	16.28	14.03 ± 0.03	13.46 ± 0.03	13.06 ± 0.03	y	y	y

Table A2 – *continued*

BPL	I_C	J_{MKO}	H_{MKO}	K_{MKO}	*IK*	*JK*	*JHK*
84	17.21	14.81 ± 0.04	14.29 ± 0.04	13.85 ± 0.04	y	y	y
89	13.89	12.01 ± 0.03	11.46 ± 0.03	11.14 ± 0.03	y	y	y
91	14.74	12.73 ± 0.03	12.21 ± 0.03	11.88 ± 0.03	y	y	y
92	15.44	13.32 ± 0.03	12.83 ± 0.03	12.44 ± 0.03	y	y	y
93	14.63	12.71 ± 0.03	12.18 ± 0.03	11.81 ± 0.03	y	y	y
94	15.26	13.58 ± 0.03	13.08 ± 0.03	12.74 ± 0.03	y	y	y
95	14.02	12.51 ± 0.03	11.96 ± 0.03	11.65 ± 0.03	y	y	y
96	16.38	14.05 ± 0.03	13.51 ± 0.04	13.13 ± 0.03	y	y	y
97	14.55	12.82 ± 0.03	12.32 ± 0.03	11.96 ± 0.03	y	y	y
98	15.82	13.95 ± 0.03	13.39 ± 0.03	13.11 ± 0.04	y	y	y
99	15.30	13.60 ± 0.03	13.08 ± 0.03	12.74 ± 0.03	y	y	y
101	16.70	14.74 ± 0.04	14.19 ± 0.05	13.82 ± 0.06	y	y	y
102	15.11	13.40 ± 0.03	12.87 ± 0.03	12.55 ± 0.03	y	y	y
103	14.57	12.90 ± 0.03	12.38 ± 0.03	12.05 ± 0.03	y	y	y
104	16.26	14.09 ± 0.03	13.54 ± 0.04	13.19 ± 0.03	y	y	y
105	15.49	13.33 ± 0.03	12.84 ± 0.03	12.43 ± 0.03	y	y	y
106	17.44	15.22 ± 0.06	14.62 ± 0.07	14.15 ± 0.07	y	y	y
107	16.18	14.04 ± 0.03	13.54 ± 0.04	13.16 ± 0.04	y	y	y
109	16.02	14.18 ± 0.03	13.70 ± 0.04	13.28 ± 0.05	y	y	y
110	16.70	14.40 ± 0.03	13.83 ± 0.04	13.47 ± 0.05	y	y	y
111	15.98	14.19 ± 0.03	13.62 ± 0.04	13.23 ± 0.04	y	y	y
112	17.30	14.98 ± 0.05	14.37 ± 0.06	14.21 ± 0.08	y	y	y
113	13.73	12.02 ± 0.02	11.45 ± 0.03	11.12 ± 0.02	y	y	y
114	13.85	12.34 ± 0.02	11.82 ± 0.03	11.48 ± 0.03	y	y	y
115	17.00	14.90 ± 0.05	14.37 ± 0.05	13.98 ± 0.06	y	y	y
116	15.79	13.75 ± 0.03	13.27 ± 0.03	12.87 ± 0.03	y	y	y
117	14.64	13.00 ± 0.03	12.49 ± 0.03	12.12 ± 0.03	y	y	y
118	14.82	13.07 ± 0.02	12.53 ± 0.03	12.17 ± 0.03	y	y	y
119	15.10	13.23 ± 0.03	12.67 ± 0.03	12.29 ± 0.04	y	y	y
120	15.06	13.11 ± 0.03	12.59 ± 0.03	12.23 ± 0.03	y	y	y
121	15.03	13.20 ± 0.03	12.67 ± 0.03	12.33 ± 0.03	y	y	y
122	17.13	14.96 ± 0.05	14.46 ± 0.06	14.04 ± 0.07	y	y	y
123	17.32	15.74 ± 0.08	14.98 ± 0.09	14.90 ± 0.15	N	y	N
125	15.80	13.98 ± 0.03	13.40 ± 0.04	13.08 ± 0.03	y	y	y
126	14.34	12.74 ± 0.02	12.18 ± 0.03	11.87 ± 0.03	y	y	y
127	17.71	15.37 ± 0.06	14.84 ± 0.07	14.32 ± 0.08	y	y	y
128	16.45	14.44 ± 0.03	13.91 ± 0.04	13.64 ± 0.05	y	y	y
129	16.23	14.23 ± 0.03	13.76 ± 0.04	13.43 ± 0.04	y	y	y
130	17.27	14.81 ± 0.04	14.27 ± 0.05	13.97 ± 0.06	y	y	y
131	16.12	14.00 ± 0.03	13.55 ± 0.04	13.18 ± 0.04	y	y	y
133	14.02	12.34 ± 0.03	11.80 ± 0.03	11.45 ± 0.03	y	y	y
134	15.60	13.62 ± 0.02	13.12 ± 0.03	12.75 ± 0.03	y	y	y
135	15.22	13.21 ± 0.04	12.73 ± 0.03	12.36 ± 0.03	y	y	y
136	15.29	13.37 ± 0.03	12.84 ± 0.03	12.46 ± 0.04	y	y	y
138	15.09	13.14 ± 0.02	12.65 ± 0.03	12.29 ± 0.03	y	y	y
139	16.23	14.07 ± 0.03	13.53 ± 0.03	13.17 ± 0.04	y	y	y
140	16.44	14.22 ± 0.04	13.71 ± 0.04	13.32 ± 0.04	y	y	y
141	14.27	12.64 ± 0.03	12.13 ± 0.03	11.78 ± 0.03	y	y	y
143	15.70	13.84 ± 0.03	13.34 ± 0.03	13.00 ± 0.03	y	y	y
144	14.06	12.30 ± 0.02	11.75 ± 0.03	11.41 ± 0.03	y	y	y
145	15.34	13.68 ± 0.03	13.17 ± 0.03	12.86 ± 0.04	y	y	y
146	16.77	14.97 ± 0.05	14.40 ± 0.06	14.21 ± 0.07	N	y	y
147	15.50	13.69 ± 0.03	13.22 ± 0.03	12.87 ± 0.03	y	y	y
148	14.93	12.97 ± 0.04	12.42 ± 0.03	12.07 ± 0.03	y	y	y
149	15.45	13.67 ± 0.03	13.10 ± 0.03	12.75 ± 0.04	y	y	y
150	15.46	13.64 ± 0.03	13.12 ± 0.03	12.74 ± 0.03	y	y	y
151	14.04	12.55 ± 0.03	12.03 ± 0.03	11.68 ± 0.03	y	y	y
153	14.76	13.03 ± 0.03	12.49 ± 0.03	12.13 ± 0.03	y	y	y
154	16.94	14.72 ± 0.04	14.20 ± 0.05	13.78 ± 0.05	y	y	y
155	15.52	13.49 ± 0.03	12.88 ± 0.03	12.54 ± 0.03	y	y	y
156	15.30	13.41 ± 0.03	12.91 ± 0.03	12.56 ± 0.04	y	y	y
157	14.78	12.95 ± 0.03	12.42 ± 0.03	12.07 ± 0.03	y	y	y
158	15.27	13.48 ± 0.03	13.01 ± 0.03	12.62 ± 0.03	y	y	y
159	13.78	12.30 ± 0.03	11.77 ± 0.03	11.45 ± 0.03	y	y	y

Table A2 – *continued*

BPL	I_C	J_{MKO}	H_{MKO}	K_{MKO}	*IK*	*JK*	*JHK*
160	15.06	12.96 ± 0.03	12.47 ± 0.04	12.12 ± 0.03	y	y	y
161	15.78	13.72 ± 0.04	13.20 ± 0.04	12.87 ± 0.03	y	y	y
162	16.07	14.15 ± 0.04	13.62 ± 0.05	13.25 ± 0.05	y	y	y
164	16.38	14.43 ± 0.04	13.96 ± 0.05	13.50 ± 0.06	y	y	y
165	14.04	11.81 ± 0.03	11.37 ± 0.04	10.97 ± 0.03	y	y	y
166	14.09	12.35 ± 0.04	11.82 ± 0.03	11.48 ± 0.03	y	y	y
167	13.74	12.13 ± 0.03	11.55 ± 0.05	11.24 ± 0.02	y	y	y
169	17.60	15.32 ± 0.06	14.71 ± 0.07	14.43 ± 0.08	y	y	y
170	15.68	13.89 ± 0.04	13.37 ± 0.05	12.97 ± 0.03	y	y	y
171	15.43	13.41 ± 0.04	12.90 ± 0.03	12.59 ± 0.03	y	y	y
173	14.16	12.42 ± 0.03	11.92 ± 0.06	11.58 ± 0.02	y	y	y
174	15.55	13.72 ± 0.04	13.26 ± 0.04	12.92 ± 0.03	y	y	y
175	14.05	12.31 ± 0.03	11.77 ± 0.03	11.48 ± 0.03	y	y	y
176	14.42	12.87 ± 0.04	12.39 ± 0.04	12.00 ± 0.04	y	y	y
177	17.06	14.86 ± 0.05	14.40 ± 0.05	14.00 ± 0.06	y	y	y
178	14.65	12.82 ± 0.03	12.31 ± 0.03	11.93 ± 0.03	y	y	y
179	15.61	15.07 ± 0.05	14.77 ± 0.07	14.56 ± 0.09	N	N	N
180	13.72	12.20 ± 0.03	11.65 ± 0.03	11.34 ± 0.03	y	y	y
181	17.33	14.73 ± 0.04	14.16 ± 0.05	13.70 ± 0.05	y	y	y
182	16.06	14.05 ± 0.03	13.52 ± 0.04	13.18 ± 0.04	y	y	y
183	16.84	14.85 ± 0.04	14.33 ± 0.05	13.84 ± 0.05	y	y	y
184	14.21	12.68 ± 0.03	12.14 ± 0.03	11.81 ± 0.03	y	y	y
185	14.86	13.18 ± 0.04	12.66 ± 0.06	12.32 ± 0.03	y	y	y
186	16.59	14.57 ± 0.04	14.06 ± 0.05	13.56 ± 0.04	y	y	y
187	14.09	12.55 ± 0.03	12.02 ± 0.03	11.67 ± 0.02	y	y	y
188	16.26	14.31 ± 0.04	13.80 ± 0.06	13.44 ± 0.04	y	y	y
189	15.22	13.45 ± 0.03	12.98 ± 0.03	12.57 ± 0.03	y	y	y
190	15.86	14.02 ± 0.04	13.50 ± 0.06	13.11 ± 0.04	y	y	y
191	17.74	15.06 ± 0.05	14.51 ± 0.06	14.08 ± 0.06	y	y	y
192	17.46	15.09 ± 0.05	14.56 ± 0.06	14.08 ± 0.06	y	y	y
193	13.73	12.10 ± 0.03	11.55 ± 0.03	11.27 ± 0.02	y	y	y
194	15.89	13.93 ± 0.04	13.45 ± 0.04	13.09 ± 0.04	y	y	y
197	16.42	14.17 ± 0.04	13.66 ± 0.04	13.33 ± 0.04	y	y	y
198	16.95	14.71 ± 0.04	14.16 ± 0.05	13.74 ± 0.05	y	y	y
206	16.43	14.16 ± 0.04	13.63 ± 0.04	13.30 ± 0.05	y	y	y
208	15.30	13.34 ± 0.04	12.79 ± 0.04	12.48 ± 0.03	y	y	y
209	14.09	12.58 ± 0.03	12.05 ± 0.03	11.73 ± 0.03	y	y	y
210	16.63	14.57 ± 0.04	14.08 ± 0.05	13.66 ± 0.05	y	y	y
211	15.99	13.88 ± 0.03	13.38 ± 0.04	13.00 ± 0.04	y	y	y
212	14.90	13.22 ± 0.03	12.69 ± 0.03	12.37 ± 0.03	y	y	y
214	17.14	14.70 ± 0.04	14.10 ± 0.04	13.69 ± 0.05	y	y	y
215	17.10	14.99 ± 0.05	14.47 ± 0.06	14.14 ± 0.06	y	y	y
216	14.76	12.91 ± 0.03	12.26 ± 0.04	11.97 ± 0.03	y	y	y
217	13.85	12.33 ± 0.03	11.83 ± 0.04	11.52 ± 0.03	y	y	y
218	17.38	15.13 ± 0.05	14.57 ± 0.06	14.36 ± 0.09	y	y	y
219	16.14	14.18 ± 0.04	13.74 ± 0.04	13.37 ± 0.05	y	y	y
220	16.46	14.39 ± 0.04	13.83 ± 0.04	13.40 ± 0.04	y	y	y
221	16.38	14.41 ± 0.04	13.93 ± 0.07	13.48 ± 0.05	y	y	y
222	14.96	13.24 ± 0.03	12.71 ± 0.04	12.35 ± 0.03	y	y	y
223	17.15	15.10 ± 0.06	14.61 ± 0.08	14.25 ± 0.09	y	y	y
224	14.71	12.85 ± 0.03	12.39 ± 0.05	12.01 ± 0.04	y	y	y
225	15.54	13.71 ± 0.03	13.26 ± 0.06	12.91 ± 0.03	y	y	y
226	14.86	13.16 ± 0.03	12.64 ± 0.04	12.37 ± 0.03	y	y	y
227	15.44	13.75 ± 0.03	13.27 ± 0.05	12.94 ± 0.03	y	y	y
228	17.37	15.05 ± 0.05	14.53 ± 0.07	14.03 ± 0.07	y	y	y
229	15.40	13.58 ± 0.03	13.03 ± 0.05	12.66 ± 0.04	y	y	y
230	14.18	12.60 ± 0.03	12.06 ± 0.06	11.70 ± 0.04	y	y	y
231	15.10	13.35 ± 0.03	12.85 ± 0.03	12.53 ± 0.03	y	y	y
232	16.02	14.20 ± 0.04	13.79 ± 0.05	13.28 ± 0.04	y	y	y

Table A2 – *continued*

BPL	I_C	J_{MKO}	H_{MKO}	K_{MKO}	*IK*	*JK*	*JHK*
233	13.70	12.27 ± 0.03	11.73 ± 0.04	11.39 ± 0.03	y	y	y
238	15.59	13.70 ± 0.03	13.11 ± 0.03	12.73 ± 0.03	y	y	y
239	15.19	13.56 ± 0.03	13.06 ± 0.03	12.69 ± 0.03	y	y	y
241	14.26	12.95 ± 0.03	12.39 ± 0.03	12.04 ± 0.03	y	y	y
242	16.11	14.26 ± 0.03	13.73 ± 0.04	13.29 ± 0.04	y	y	y
243	13.97	12.42 ± 0.03	11.86 ± 0.03	11.47 ± 0.03	y	y	y
244	14.29	12.64 ± 0.03	12.11 ± 0.03	11.72 ± 0.02	y	y	y
245	15.07	13.49 ± 0.03	12.96 ± 0.03	12.58 ± 0.03	y	y	y
246	15.16	13.60 ± 0.03	13.03 ± 0.03	12.74 ± 0.04	y	y	y
247	16.90	15.21 ± 0.06	14.57 ± 0.06	14.20 ± 0.07	N	y	y
248	15.16	13.45 ± 0.03	12.95 ± 0.03	12.63 ± 0.04	y	y	y
250	15.49	13.61 ± 0.03	13.17 ± 0.03	12.80 ± 0.04	y	y	y
251	15.57	13.84 ± 0.03	13.29 ± 0.04	12.95 ± 0.04	y	y	y
252	15.38	13.80 ± 0.03	13.29 ± 0.03	12.91 ± 0.04	y	y	y
253	17.24	15.26 ± 0.05	14.63 ± 0.06	14.25 ± 0.07	y	y	y
255	16.07	14.11 ± 0.03	13.64 ± 0.03	13.28 ± 0.04	y	y	y
260	15.73	13.97 ± 0.03	13.48 ± 0.04	13.07 ± 0.04	y	y	y
264	14.98	13.41 ± 0.03	12.86 ± 0.03	12.49 ± 0.04	y	y	y
267	16.41	14.61 ± 0.04	14.06 ± 0.05	13.67 ± 0.05	y	y	y
272	16.53	14.74 ± 0.04	14.14 ± 0.05	13.70 ± 0.06	y	y	y
276	14.01	13.17 ± 0.03	12.84 ± 0.03	12.70 ± 0.04	N	N	N
280	16.75	14.77 ± 0.04	14.32 ± 0.06	13.79 ± 0.06	y	y	y
281	15.79	14.09 ± 0.03	13.55 ± 0.04	13.16 ± 0.04	y	y	y
285	14.97	13.36 ± 0.03	12.83 ± 0.03	12.52 ± 0.04	y	y	y
290	14.71	13.14 ± 0.03	12.60 ± 0.03	12.27 ± 0.03	y	y	y
291	16.40	14.37 ± 0.04	13.83 ± 0.04	13.44 ± 0.05	y	y	y
292	16.73	14.96 ± 0.05	14.46 ± 0.06	14.15 ± 0.07	N	y	y
293	17.16	15.17 ± 0.05	14.67 ± 0.07	14.28 ± 0.08	y	y	y
296	16.79	15.07 ± 0.05	14.50 ± 0.06	14.11 ± 0.07	N	y	y
298	14.20	12.66 ± 0.03	12.16 ± 0.03	11.81 ± 0.03	y	y	y
299	16.61	14.74 ± 0.04	14.24 ± 0.05	13.84 ± 0.05	y	y	y
301	15.58	13.85 ± 0.03	13.30 ± 0.03	12.93 ± 0.03	y	y	y
305	14.07	12.62 ± 0.03	12.10 ± 0.03	11.74 ± 0.02	y	y	y
310	14.44	12.90 ± 0.03	12.36 ± 0.04	12.06 ± 0.04	y	y	y
311	14.96	13.41 ± 0.03	12.85 ± 0.03	12.54 ± 0.03	y	y	y
313	16.44	14.55 ± 0.04	13.99 ± 0.05	13.74 ± 0.05	y	y	y
314	13.82	12.65 ± 0.03	12.07 ± 0.03	11.78 ± 0.03	N	y	y
318	13.88	12.61 ± 0.03	12.00 ± 0.03	11.74 ± 0.03	N	y	y
319	13.75	12.87 ± 0.03	12.44 ± 0.03	12.28 ± 0.03	N	N	N
320	15.59	14.02 ± 0.03	13.50 ± 0.03	13.15 ± 0.03	y	y	y
321	14.41	12.91 ± 0.03	12.30 ± 0.03	11.93 ± 0.04	y	y	y
322	15.86	14.19 ± 0.03	13.68 ± 0.03	13.25 ± 0.04	y	y	y
323	16.27	14.38 ± 0.03	13.93 ± 0.04	13.56 ± 0.04	y	y	y
324	14.15	12.77 ± 0.03	12.21 ± 0.03	11.84 ± 0.03	y	y	y
325	17.41	15.21 ± 0.05	14.81 ± 0.07	14.28 ± 0.08	y	y	y
326	16.96	15.06 ± 0.04	14.50 ± 0.05	14.27 ± 0.08	N	y	y
327	18.00	15.52 ± 0.05	14.93 ± 0.07	14.78 ± 0.12	y	y	y
328	16.95	14.72 ± 0.04	14.10 ± 0.04	13.68 ± 0.05	y	y	y
329	14.52	13.05 ± 0.03	12.47 ± 0.03	12.15 ± 0.03	y	y	y
330	15.73	14.16 ± 0.03	13.57 ± 0.03	13.23 ± 0.04	y	y	y
331	17.67	15.41 ± 0.05	14.75 ± 0.06	14.34 ± 0.09	y	y	y
332	16.41	14.59 ± 0.04	14.04 ± 0.05	13.66 ± 0.05	y	y	y
333	14.69	13.02 ± 0.03	12.45 ± 0.03	12.13 ± 0.03	y	y	y
334	17.47	15.27 ± 0.05	14.67 ± 0.06	14.31 ± 0.08	y	y	y
335	15.36	13.55 ± 0.03	13.05 ± 0.04	12.66 ± 0.03	y	y	y
336	17.46	15.30 ± 0.05	14.70 ± 0.06	14.26 ± 0.08	y	y	y
337	16.71	14.69 ± 0.04	14.15 ± 0.04	13.73 ± 0.05	y	y	y
338	16.81	15.07 ± 0.04	14.52 ± 0.05	14.24 ± 0.07	N	y	y
339	13.84	12.43 ± 0.03	11.88 ± 0.03	11.46 ± 0.03	y	y	y

Table A3. Photometry (c2–5), membership (c6–8) and binarity (c9) of RIZ-Pr Praesepe candidates. Membership is from the *IK* CMD, the *JK* CMD and the *JHK* diagram.

RIZ-Pr	I_C^a	J_{MKO}	H_{MKO}	K_{MKO}	*IK*	*JK*	*JHK*	Bin
1	20.14	17.06 ± 0.05	16.47 ± 0.04	16.14 ± 0.08^b	y	y	y	
2†	18.19	15.67 ± 0.05	15.11 ± 0.03	14.77 ± 0.04^b	y	y	y	b
3	21.20	19.05 ± 0.17	18.01 ± 0.12	16.77 ± 0.08	y	N	N	
4	18.52	16.04 ± 0.03	15.56 ± 0.03	15.23 ± 0.04^b	y	y	y	
5	20.86	19.09 ± 0.17	18.20 ± 0.16	16.94 ± 0.06	y	N	N	
6	21.09	19.10 ± 0.18	18.11 ± 0.16	17.07 ± 0.08 17.01 ± 0.07 17.32 ± 0.05^b	y	N	N	
7	21.24	–	–	18.56 ± 0.29 19.15 ± 0.05^b	N	–	–	
8	17.81	15.40 ± 0.05	14.89 ± 0.03	14.60 ± 0.04^b	y	y	y	
9	21.25	–	–	17.72 ± 0.13	N	–	–	
10	20.54	–	–	18.08 ± 0.07^b	N	–	–	
11	19.47	16.66 ± 0.05	16.23 ± 0.04	15.84 ± 0.14^b	y	y	y	
12	20.10	–	–	16.91 ± 0.21^b	N	–	–	
13	20.24	–	–	19.04 ± 0.50 18.49 ± 0.11^b	N	–	–	
14	20.59	–	–	17.82 ± 0.06^b	N	–	–	
15	21.36	–	–	18.49 ± 0.27	N	–	–	
16	21.10	–	–	18.60 ± 0.31	N	–	–	
17	20.41	18.23 ± 0.10	17.65 ± 0.12	17.28 ± 0.11	N	N	y	
18	19.63	16.40 ± 0.04	15.74 ± 0.03	15.40 ± 0.04^b	y	y	N?	b
19	21.42	–	–	18.04 ± 0.18	N	–	–	
20	18.48	16.16 ± 0.04	15.57 ± 0.03	15.19 ± 0.04^b	y	y	y	
21‡	18.73	15.89 ± 0.03	15.39 ± 0.03	15.03 ± 0.03^b	y	y	y	b
22	21.55	–	–	n-d	N	–	–	
23	19.06	16.63 ± 0.04	16.04 ± 0.03	15.53 ± 0.03 15.98 ± 0.16^b	y	y	y	b
24	20.43	17.30 ± 0.05	16.68 ± 0.04	16.17 ± 0.06 16.19 ± 0.03^b	y	y	y	b
25	21.20	–	–	18.62 ± 0.31	N	–	–	
26	18.08	–	–	15.49 ± 0.04^b	N	–	–	

Refs: (a) Pinfield et al. (1997), (b) Hodgkin et al. (1999). The † is also IZ-Pr 40. The ‡ is also IZ-Pr 86. n-d = non-detection.

Table A4. Photometry (c2–5), membership (c6–8) and binarity (c9) of IZ-Pr Praesepe candidates. Membership is from the *IK* CMD, the *JK* CMD and the *JHK* diagram.

IZ-Pr	I_C^a	J_{MKO}	H_{MKO}	K_{MKO}	*IK*	*JK*	*JHK*	Bin
1	18.02	15.60 ± 0.03	15.13 ± 0.05	14.72 ± 0.03	y	y	y	b
2	17.25	15.44 ± 0.03	14.94 ± 0.05	14.64 ± 0.03	y	y	y	
3	18.19	15.87 ± 0.03	15.36 ± 0.05	15.09 ± 0.02	y	y	y	
4	18.21	16.56 ± 0.13^b	15.76 ± 0.13^b	15.31 ± 0.06	y	y	?	
5	18.33	–	–	15.83 ± 0.03	N	–	–	
6	17.26	15.62 ± 0.06^b	15.15 ± 0.08^b	14.79 ± 0.03	y	y?	?	
7	19.90	–	–	16.52 ± 0.05	N	–	–	
8	17.22	15.57 ± 0.06^b	15.16 ± 0.08^b	14.72 ± 0.03	y	y?	?	
9	20.37	–	–	17.66 ± 0.12	N	–	–	
10	18.26	15.79 ± 0.03	15.30 ± 0.05	14.95 ± 0.02	y	y	y	b
11	17.47	15.63 ± 0.03	15.10 ± 0.05	14.82 ± 0.03	y	y	y	
12	19.93	–	–	17.36 ± 0.09	N	–	–	
13	19.14	–	–	16.08 ± 0.04	N	–	–	
14	17.84	16.03 ± 0.07^b	15.50 ± 0.09^b	15.02 ± 0.03	y	y	?	
15	17.94	16.08 ± 0.08^b	15.63 ± 0.09^b	15.11 ± 0.03	y	y	?	
16	17.18	–	–	14.99 ± 0.03	N	–	–	
17	17.61	15.74 ± 0.03	15.24 ± 0.05	14.86 ± 0.03	y	y	y	
18	18.54	16.18 ± 0.03	15.81 ± 0.03	15.30 ± 0.04	y	y	N	
19	19.93	–	–	16.78 ± 0.06	N	–	–	
20	17.22	15.43 ± 0.03	14.92 ± 0.05	14.58 ± 0.03	y	y	y	
21	19.72	–	–	17.19 ± 0.08	N	–	–	
22	19.65	–	–	16.18 ± 0.04	y	–	–	
23	19.20	16.47 ± 0.03	16.04 ± 0.03	15.57 ± 0.04	y	y	y	
24	17.52	15.47 ± 0.03	14.95 ± 0.05	14.56 ± 0.03	y	y	y	b
25	17.98	15.49 ± 0.03	14.94 ± 0.05	14.64 ± 0.02	y	y	y	b
26	17.38	15.30 ± 0.03	14.86 ± 0.04	14.52 ± 0.03	y	y	y	

Table A4 – *continued*

IZ-Pr	I_C^a	J_{MKO}	H_{MKO}	K_{MKO}	*IK*	*JK*	*JHK*	Bin
27	19.81	–	–	16.77 ± 0.06	N	–	–	
28	17.89	16.22 ± 0.09^b	15.50 ± 0.09^b	15.15 ± 0.03	y	y	?	
29	19.62	–	–	16.90 ± 0.06	N	–	–	
30	17.55	15.51 ± 0.03	15.09 ± 0.05	14.72 ± 0.03	y	y	y	
31	17.41	15.38 ± 0.03	14.91 ± 0.02	14.54 ± 0.03	y	y	y	
32	19.19	–	–	15.88 ± 0.03	y	?	–	
33	17.30	15.36 ± 0.03	14.90 ± 0.05	14.55 ± 0.03	y	y	y	
34	19.34	–	–	17.49 ± 0.10	N	–	–	
35	19.77	–	–	16.50 ± 0.05	N	–	–	
36	19.41	16.62 ± 0.04	16.11 ± 0.03	15.66 ± 0.02	y	y	y	
37	19.28	–	–	16.40 ± 0.04	N	–	–	
38	18.22	–	–	15.52 ± 0.03	N	–	–	
39	19.44	–	–	16.58 ± 0.05	N	–	–	
40†	18.04	15.74 ± 0.04	15.08 ± 0.03	14.79 ± 0.04	y	y	y	
41	18.02	15.75 ± 0.04	15.28 ± 0.02	14.83 ± 0.03	y	y	y	b
42	20.33	–	–	17.03 ± 0.08	N	–	–	
43	19.47	–	–	16.09 ± 0.10	y	–	–	
44	17.49	15.76 ± 0.06^b	15.32 ± 0.08^b	14.84 ± 0.04	y	y	?	
45	17.18	–	–	15.46 ± 0.11	N	–	–	
50	18.29	–	–	15.43 ± 0.03	y	–	–	
52	19.21	–	–	16.27 ± 0.04	N	–	–	
54	17.67	15.87 ± 0.08^b	15.39 ± 0.10^b	15.07 ± 0.14^b	y	y?	?	
55	17.40	15.74 ± 0.07^b	15.18 ± 0.08^b	15.15 ± 0.15^b	N	N	?	
56	17.38	15.51 ± 0.06^b	14.93 ± 0.07^b	14.53 ± 0.09^b	y	y	?	
57	17.45	15.62 ± 0.06^b	15.01 ± 0.07^b	14.62 ± 0.09^b	y	y	?	
59	18.47	–	–	15.83 ± 0.04	N	–	–	
60	17.48	15.60 ± 0.06^b	15.20 ± 0.09^b	14.81 ± 0.11^b	y	y?	?	
61	17.59	16.07 ± 0.09^b	15.38 ± 0.10^b	14.99 ± 0.13^b	y	y	?	
62	17.77	16.07 ± 0.09^b	15.55 ± 0.11^b	15.11 ± 0.14^b	y	y	?	
63	17.42	15.72 ± 0.06^b	14.99 ± 0.08^b	14.51 ± 0.08^b	y	y	?	b
64	17.44	15.30 ± 0.05^b	14.66 ± 0.06^b	14.19 ± 0.06^b	y	y	?	b
66	17.26	15.40 ± 0.05^b	14.81 ± 0.07^b	14.61 ± 0.09^b	y	y?	?	
69	17.30	15.45 ± 0.05^b	14.89 ± 0.07^b	14.53 ± 0.09^b	y	y	?	
70	17.32	15.40 ± 0.05^b	14.74 ± 0.07^b	14.53 ± 0.09^b	y	y?	?	
72	17.29	15.38 ± 0.05^b	14.93 ± 0.07^b	14.36 ± 0.09^b	y	y	?	b
74	17.87	15.89 ± 0.07^b	15.06 ± 0.08^b	14.90 ± 0.12^b	y	y	?	
77	17.41	15.71 ± 0.06^b	15.14 ± 0.08^b	14.76 ± 0.10^b	y	y	?	
80	17.37	15.55 ± 0.05^b	14.81 ± 0.07^b	14.52 ± 0.08^b	y	y	?	
82	19.24	–	–	16.54 ± 0.04	N	–	–	
84	17.99	15.95 ± 0.07^b	15.26 ± 0.08^b	15.13 ± 0.14^b	y	y?	?	
85	18.92	–	–	17.03 ± 0.05	N	–	–	
86‡	18.63	15.89 ± 0.03	15.39 ± 0.03	15.01 ± 0.03	y	y	y	
88	17.98	16.11 ± 0.09^b	15.85 ± 0.15^b	15.15 ± 0.15^b	y	y	?	
93	19.29	16.76 ± 0.04	16.21 ± 0.03	15.75 ± 0.03	y	y	y	
94	18.25	16.02 ± 0.10^b	15.44 ± 0.11^b	15.00 ± 0.03	y	y	–	b
95	19.47	–	–	16.78 ± 0.03	N	–	–	
97	19.50	–	–	16.75 ± 0.04	N	–	–	
99	17.86	15.88 ± 0.09^b	15.19 ± 0.10^b	14.98 ± 0.13^b	y	y	?	
100	17.34	15.40 ± 0.06^b	14.95 ± 0.09^b	14.59 ± 0.08^b	y	y?	?	
104	19.50	–	–	16.84 ± 0.06	N	–	–	
105	18.80	–	–	16.15 ± 0.03	N	–	–	
108	17.31	15.47 ± 0.06^b	14.83 ± 0.07^b	14.57 ± 0.10^b	y	y	?	
110	18.68	–	–	16.74 ± 0.05	N	–	–	
112	17.89	16.01 ± 0.09^b	15.53 ± 0.12^b	15.17 ± 0.15^b	y	y?	?	
113	18.44	16.03 ± 0.03	15.58 ± 0.03	15.17 ± 0.03	y	y	y	
117	19.09	16.56 ± 0.04	16.02 ± 0.03	15.70 ± 0.03	y	y	y	
119	17.94	15.77 ± 0.08^b	15.00 ± 0.08^b	14.66 ± 0.09^b	y	y	?	b
120	17.48	15.68 ± 0.07^b	15.28 ± 0.09^b	14.75 ± 0.11^b	y	y	?	
123	19.49	15.79 ± 0.08^b	15.41 ± 0.11^b	15.26 ± 0.15^b	y	N	?	
125	17.48	16.01 ± 0.09^b	15.52 ± 0.11^b	15.21 ± 0.15^b	N	y?	?	
126	18.79	15.94 ± 0.09^b	15.57 ± 0.12^b	15.22 ± 0.02	y	y?	?	b
127	19.98	16.48 ± 0.16^b	16.18 ± 0.23^b	15.49 ± 0.19^b	y	y	?	
128	17.50	15.57 ± 0.07^b	14.89 ± 0.08^b	14.62 ± 0.09^b	y	y	?	

Refs: (a) Pinfield et al. (2000), (b) 2MASS. The † is also RIZ-Pr 2. The ‡ is also RIZ-PR 21.

This paper has been typeset from a TEX/LATEX file prepared by the author.